

A computational scheme to evaluate Hamaker constants of molecules with practical size and anisotropy

Kenta Hongo* and Ryo Maezono

School of Information Science, JAIST, Asahidai 1-1, Nomri, Ishikawa 923-1292, Japan[†]

(Dated: September 17, 2018)

We propose a computational scheme to evaluate Hamaker constants, A , of molecules with practical sizes and anisotropies. Upon the increasing feasibility of diffusion Monte Carlo (DMC) methods to evaluate binding curves for such molecules to extract the constants, we discussed how to treat the averaging over anisotropy and how to correct the bias due to the non-additivity. We have developed a computational procedure for dealing with the anisotropy and reducing statistical errors and biases in DMC evaluations, based on possible validations on predicted A . We applied the scheme to cyclohexasilane molecule, Si_6H_{12} , used in 'printed electronics' fabrications, getting $A \sim 105 \pm 2$ [zJ], being in plausible range supported even by other possible extrapolations. The scheme provided here would open a way to use handy *ab initio* evaluations to predict wettabilities as in the form of materials informatics over broader molecules.

INTRODUCTION

Hamaker constants [1], A , dominate the wettability [2, 3] of solvents, which is one of the critical properties in industrial applications of Sol-Gel methods [4], including solution processes for semiconductor devices. [5] Microscopic insights on the wettability [2, 3] relates the Hamaker constant with molecular interactions, which can be, in principle, evaluated from *ab initio* simulations. From the asymptotic behavior of molecular binding curves, or potential energy surfaces (PES), $\sim C_6/R^6$, the Hamaker constant can be computed as $A_{\text{add}} = \pi C_6 \rho^2$, provided that only a binding with a single C_6 matters and a naive superposition is expected. [3] The index, 'add', then stands for 'additive' and ρ denotes the molecular density which appears when the superposition integral is counted. Though we can find several such prototypical works [3] of the '*ab initio* assessment' applied to simple and highly symmetric molecules, we would immediately encounter troubles when attempting to apply the framework to practical solute molecules. Most molecules of industrial interest are not so highly symmetric that we cannot generally expect the additivity of the interaction. [6] In these cases, too many alignments of coalescence are possible due to the anisotropy of molecules, bewildering us how to model the coalescence with the confidence for capturing the nature of the system.

The main subject of the present paper is how to estimate A for the practical solute molecules via A_{add} with plausible considerations mainly for the anisotropy. Once we could establish such a scheme, such database of molecular interactions aided by recent *ab initio* methods [7, 8] can provide the Hamaker constants over various liquids. It would help to predict, control, and design such solution processes including not only wettabilities but also suspensions and solvabilities by using empirical molecular dynamics simulations. [2]

The present study has been originally motivated by the demand to estimate A for a cyclohexasilane molecule,

Si_6H_{12} (CHS), which is used as an ink for 'printed electronics' technology to fabricate polycrystalline Si film transistors. [5] The ink including Si-based precursors is sprayed on a substrate, which is sintered to form an amorphous Si thin film, without using expensive vacuum equipment in the conventional semiconductor processes. The ink printing process has hence attracted recent interests for realizing more saving and lower environmental impact technology. [5] Controlling the wettability of these inks is of rather general interest because the technology is about to be applied further to fabricate oxide or carbon nanotube film semiconductor devices [9, 10] by using various inks instead of Si-based ones. For going beyond conventional/experimental preparations of inks, several simulations have been made to analyze the wettability of droplets on ink-jet processes dynamically using molecular dynamics [11] or empirical models [12]. The predictability of these simulations strongly depends on the force fields that are currently prepared by empirical parameterizations of Lennard-Jones type potentials. The *ab initio* assessment for these parameterizations is obviously recognized as an important breakthrough in getting more universal applicability.

For CHS, there is no reference to A , and then we tried evaluating A_{add} from its binding curve. Besides the anisotropy discussed above, the commonly available framework, DFT (density functional theory), is known to fail to describe molecular interactions mostly, and the DFT performance strongly depends on exchange-correlation (XC) functionals adopted. [13] In the present case, the interaction of this system, CHS, is of non- π staking nature, known as an *aliphatic-aliphatic* one [14] between the σ bonds at the HOMO (highest-occupied molecular orbital) levels of the monomers. Unlike *aromatic-aromatic* interactions of *e.g.* benzene dimer, there has been only a few investigations on *aliphatic-aliphatic* interactions and hence no established scheme of how to treat the anisotropy of molecules in the evaluation of binding curves even for moderately tractable size and

symmetry of the target molecules. As is well-known, accurate correlated methods such as CCSD(T) are required to get enough reliable estimations of molecular interaction. [13, 15] Such methods are, in general, quite costly in the sense of the scalability on the system size N , *e.g.*, $\sim N^7$ for CCSD(T) [16]. Such severe scalabilities obstruct the applications to larger molecules being likely in the practical cases. In contrast, DMC (diffusion Monte Carlo) method is quite promising and its applicability to more practical issues gets rapidly extended. [17–20] This framework is regarded in principle as the most reliable that can achieve ‘numerically exact solutions’ in some cases [21, 22], and there has been so far several applications to noncovalent systems [23–33], to calibrate even over accurate molecular orbital methods such as CCSD(T). DMC scales at worst to $\sim N^3$, [18] making it possible to be applied further to larger molecules including molecular crystals. [28–32]

In this paper, we therefore applied DMC to evaluate A_{add} of CHS. Upon a careful benchmark on benzene molecule (given in Appendix C), we have established a scheme (i) coping with the anisotropy of the molecules, (ii) reducing statistical errorbars and biases that are small enough for a usable predictions, and (iii) based on several possible validations on the predicted A for which no experimental reference value is available. The scheme is applied to CHS getting $A = 105 \pm 2$ [zJ] which is in a reasonable range validated by several side considerations. By making comparisons with binding curves by DFT, we also provide a useful calibration over several XC for the predictability of A .

The paper is then organized as follows: In the main body of the paper, we provide descriptions of the scheme applied to CHS, followed by validations of the prediction as briefly as possible so as to concentrate on following the established procedure. Thus, put aside into appendices are detailed descriptions for computational methods (Appendix A), some formalism of Hamaker constants considered in the present work (Appendix B), and all the discussions on the validations of the procedure made on the benzene dimer benchmark (Appendix C-E). Technical details about evaluation of A_{add} for CHS are also given alongside the benzene case in the appendices. Summaries of the paper are given as Concluding Remarks at the end of main text. For detailed correction schemes, such as BSSE (basis set superposition error), CBS (complete basis set) schemes as well as time-step error in DMC are given in Supporting Information.

RESULTS AND DISCUSSIONS

Hamaker constant of CHS

To get C_6 , we evaluated dimer binding curves of CHS for three types of coalescences, *i.e.*, Sandwich (Type-A),

T-shape (Type-B), and Parallel (Type-C), as shown in Fig. 1. Computational details for the evaluation are given in Appendix A. For the CHS monomer structure, we took the chair conformation [34, 35] since it is known to be most stable. The monomer geometry is optimized at the B3LYP/6-311G level using Gaussian09. [36] To plot a binding curve, we vary binding distances of a dimer coalescence, keeping each of the monomer structures fixed to the above one. This is valid to some extent because we focus on C_6 extracted from the long-range behavior where each of the monomer structures may be almost the same as that of an isolated monomer. The inter-monomer distance is defined as that between the centers of gravity of the monomers.

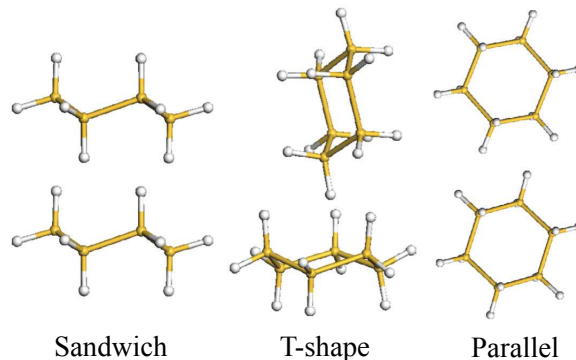


FIG. 1. Typical configurations of the dimer coalescence considered in this work, Sandwich (Type-A), T-shaped (Type-B), and Parallel (Type-C).

Fig. 2 shows DMC binding curves for each coalescence configurations, compared with CCSD(T) references. The sandwich (Type A) configuration is identified to give the most stable binding energy ΔE over the others, $p \sim \exp(-\Delta E/kT) \sim 98\%$ at $T = 298.15\text{K}$ as given in Table I. Our careful benchmark for benzene case given in Appendix C clarifies that the deepest binding configuration almost dominates Hamaker constants. We can therefore concentrate only on the Type A binding curve to extract C_6 from its asymptotic behavior. Hereafter we adopt a symbol, C_6^{stable} , as a C_6 value for the most stable coalescence configuration.

To extract C_6^{stable} from PES data, we considered several fitting schemes: log-fit, 6-12 Lennard-Jones (LJ), and the power-fit for the correlation energy defined as the deviation from Hartree-Fock energy (denoted as $C_6^{\text{stable;LOG}}$, $C_6^{\text{stable;LJ}}$, and $C_6^{\text{stable;Corr}}$). The estimation is also affected by the choice of which distance range is taken to be fit. We make detailed discussions of our fitting schemes in Appendix D, considering the benzene benchmark as well as CHS. From them, we find out that

	B3LYP-GD3	MP2	CCSD(T)	DMC
$p(A)/R_e$	0.971/4.9	0.976/4.7	0.968/4.8	0.987(82)/4.83(2)
$p(B)/R_e$	0.026/6.6	0.023/6.1	0.030/6.2	0.010(24)/6.37(6)
$p(C)/R_e$	0.003/8.8	0.002/8.4	0.003/8.6	0.003(14)/8.7(1)
\bar{R}_{dim}	5.0	4.7	4.9	4.9(1)

TABLE I. Comparisons of the equilibrium stability among three coalescence configurations in Fig. 1, in terms of the thermal probability weight, $p \sim \exp(-\Delta E/kT)$. Equilibrium binding lengths, R_{eq} [\AA], are also shown. \bar{R}_{dim} [\AA] is the thermal averaged binding lengths at $T = 298.15$ K for each method.

the power-fit for the correlation energy [37, 38]

$$\Delta E_{\text{corr}}(R) = -\frac{C_6}{R^6} - \frac{C_8}{R^8} \dots, \quad (1)$$

achieves small enough errorbars for usable predictions on the Hamaker constant by DMC, $A_{\text{add}}(C_6^{\text{stable};\text{Corr}}) = 105 \pm 2$ [zJ], with the fitting range $R = 4.4 \sim 6.4 \text{\AA}$ which minimizes a measure of the deviation from the fitting model (Appendix D), where the experimental density of CHS, $\rho = 0.323 \times 10^{28} [\text{1/m}^3]$ at 298.15K. [39] was used to evaluate $A_{\text{add}} = \pi \rho^2 C_6$. We note that this scheme is applicable only to many-electron wavefunction methods such as DMC, CCSD(T), and MP2. The Hamaker constants evaluated from various approaches (methods/schemes) in the present study are listed in Table II, and their validation is given in the next subsection.

Validation of A value

We found that our DMC evaluations of A_{add} agree with those obtained from the other reliable quantum chemistry methods, CCSD(T) and MP2, implying our *ab-initio* evaluation schemes would be reasonable within the framework of many-electron wavefunction theory. But, there is no reference to A to be compared directly to the present estimation for CHS. So we tried a validation via side-way manner as follows: (1) A simple estimation using London's theory [37] would give underestimated reference as discussed in Appendix C. Static polarizabilities and ionization energies can be evaluated using HF and B3LYP levels of theory to give C_6 values (denoted as $\langle C_6^{\text{London}} \rangle_{\text{iso}}$) and then $A_{\text{add}}(\langle C_6^{\text{London}} \rangle_{\text{iso}}) = 66$ and 81 [zJ], respectively ($\langle \dots \rangle_{\text{iso}}$ means an isotropic orientation average, described in Appendix B and C). The values are consistent in the sense that they are actually located in the underestimated range compared with the other estimations in Table II.

(2) As another trial for the validation using the estimations (A_L) based on the Lifshitz theory [40] whose formalism is given in Appendix B, we consider the dependence on the molecular weights of $A \propto C_6$. Since the dispersion interactions scale to the total polarization, it is not so bad expectation that A is roughly proportional to molecular weights. Under this assumption, the

ratio, $A_L(C_6H_{12})/A_L(C_5H_{10}) = (53.0 \pm 0.2)/(49.4 \pm 0.3)$, can be taken as being equal to $A_L(\text{Si}_6\text{H}_{12})/A_L(\text{Si}_5\text{H}_{10})$. Using the known value of A_L (73.4 ± 0.4 zJ) for CPS(Si_5H_{10}), we can roughly estimate that of CHS as $A_L(\text{extrapol.}) = 78.9 \pm 0.5$ [zJ]. Another possible regression can be made in terms of C_6 instead of A . Regressing the quadratic functions to the TDDFT and EMT (effective medium theory) data on C_6 values of the Si_nH_m family [41] (denoted as $C_6^{\text{extrapol.}}$), we get $A_{\text{add}}(C_6^{\text{extrapol.}}) = 110$ [zJ] and 94 [zJ], respectively. These values lie within a reasonable range by comparison with those in Table II, being consistent with the fact that A_{add} is larger than $A_L(\text{extrapol.})$. We found the EMT extrapolation of A_{add} being closer to $A_L(\text{extrapol.})$. This may be attributed to the fact that, in EMT, C_6 is evaluated by the dielectric constants modelled by those of bulk quantities, as in the Lifshitz theory. The reason why A_{add} generally overestimates A values compared with A_L may be explained as follows: $A_{\text{add}}(C_6^{\text{stable}})$ is evaluated only from the longest-ranged exponent with a selected coalescence configuration, Type-A in the present case. The other configurations with shorter-ranged exponents should be included in liquids by some fractions, and hence effectively weaken the binding strength estimated under such an assumption with 100% constitution of Type-A coalescence. Such an effect would be represented as 'effectively reduced' Hamaker constants close to A_L . Hence, the values, A_{add}/A_L , could be sorted out by a factor dominating the fraction, $\exp(-\Delta E/kT)$, where ΔE denotes a typical energy difference between the coalescence configurations with the longest- and the shortest-ranging exponents.

Validation of equilibrium properties

Although the long-range behavior of PES concerns with the evaluation of A , validation of PES at equilibrium distance may also give us some confidence in our numerical results. Equilibrium properties including binding energies (ΔE) and equilibrium lengths (R_{eq}) are summarized in Table III. The estimated binding energies in our DMC-PES are comparable with the typical value of non- π stacking energies ~ -5 kcal/mol. [14] Compared with π -stacking energies, it is about twice larger, which would be consistent with the higher boiling temperature

Method/Scheme	LOG	LJ	Corr	London
LDA	48	90		
M06-2X	36	56		
B3LYP				81 ^a
B3LYP-GD2	57	62		
B3LYP-GD3	96	105		
B97-D	98	81		
HF				66 ^b
MP2	104	99	104	
CCSD(T)	95	103	106	
DMC	99(30)	107(7)	105(2)	

TABLE II. Computed Hamaker constants $A_{\text{add}}(C_6^{\text{stable}})$ [zJ], based on different C_6 evaluation schemes, $C_6^{\text{stable;LOG}}/C_6^{\text{stable;LJ}}/C_6^{\text{stable;Corr}}$ (see text for more details about the definitions). Since HF and B3LYP give repulsive PESs, their Hamaker constants cannot be evaluated by the present PES scheme, and the London scheme is used to estimate $A_{\text{add}}((C_6^{\text{London}})^{\text{iso}})$, instead. Statistical errors in the DMC values are given in parenthesis.

of CHS than that of its structural isomers with the same molecular weights but without hydrogen bindings. [42]

For further possible validations of our DMC-PES, we would take the facts that (a) The PESs are consistent with those estimated by another reliable standard, CCSD(T), and (b) We can make a plausible comparison that explains the experimentally observed density from our estimated binding lengths R_e . For (a), we provide detailed discussions on the comparison as well with DFT later (see ‘‘Calibration of DFT’’).

As for (b), our scheme that relates R_e with an experimental density is confirmed to work well not only for CHS but also for benzene molecules as described in Appendix E. For CHS, experimental values of the molecular weight (180.61 g/mol) and density (0.97 g/cm³ at $T = 298.15\text{K}$) lead to the mean inter-molecular distance, $R_\rho = 6.8 \text{ \AA}$, which fairly reasonably drops within the binding lengths of Type-A to C. As shown in Table I, the simple thermal averaging over the three configurations by the factor $p \sim \exp(-\Delta E/kT)$ gives us an underestimation $\bar{R}_{\text{dim}} \sim 4.9 \text{ \AA}$ compared with R_ρ . An alternative averaging over the ‘diagonal lengths’ of four-body trapezoids, as shown in Fig. 3, gives an improved estimate, \bar{R}_{tetra} , getting closer to the experimental estimation of 6.8Å, as shown in Table IV.

Calibration of DFT

DFT is a much more practical choice of methods combined with our *ab initio* Hamaker evaluation schemes, but its reliability strongly depends on XC functionals adopted as usual. Here we provide a useful calibration over several XC functionals appropriate for predicting A values, by comparing with the many-electron wavefunction theories.

Fig. 4 highlights typical binding curves evaluated by various methods, though only for Type-A (for the other

types, see Supporting Information). All the SCF curves were corrected by the BSSE scheme [16, 43–45] (see Supporting Information). The present study takes CCSD(T) as a standard reference to calibrate the performance of the SCF approaches. We can find the DFT predictions scattering around CCSD(T). Except LDA, conventional functionals such as PBE and B3LYP fail to capture the binding itself. The LDA overbinding has been frequently reported for several molecular bindings. [28–31, 46] This can be regarded as spurious due to improper self interactions: Exchange repulsion is not fully reproduced in LDA because of the lack of the exact cancellation of self interaction, and hence spurious ‘chemical’ bindings are formed due to the weakened repulsions, rather than true molecular bindings. The exchange repulsion weakened in LDA gets recovered when changing XC into GGA and further into B3LYP, which may explain the repulsive curves pushing the minimum toward distant region. As LDA is known to inherently fail to describe dispersion interactions, a significant difference in the LDA estimations between $A_{\text{add}}(C_6^{\text{stable;LOG}})$ and $A_{\text{add}}(C_6^{\text{stable;LJ}})$ (see Table II) implies a poor reliability on its long-range behavior description.

The XC functionals for molecular interactions, M06-2X, B97-D and B3LYP-GD(2,3), on the other hand, well reproduce the bindings at their equilibrium lengths, as seen in Fig. 4. We see, however, that M06-2X and B3LYP-GD2 give rise to less reliable asymptotic behaviors at long-range region, where they decay much faster than CCSD(T) or the other XC functionals for molecular interactions. As for M06-2X, its functional form based on hybrid meta-GGA does not explicitly contain dispersion interactions by its construction, and its parameterizations of the XC functionals are adjusted so as to reproduce a number of molecular bindings *around* their equilibrium geometries, giving rise to the unreliable long-range behavior. B97-D and B3LYP-GD2 are classified into the DFT-D2 family including ‘atom-pairwise’

	Equilibrium properties		Short-range	Long-range
	$\Delta E(R_e)$	\bar{R}_e	$\Delta E(4.2)$	$\Delta E(7.0)$
LDA	-9.39[NG]	4.34[NG]	-8.73[NG]	-0.44[NG]
B3LYP-GD2	-3.47[NG]	4.93[G]	2.09[NG]	-0.71[NG]
B3LYP-GD3	-5.06[G]	4.93[G]	5.74[NG]	-1.13[G]
B97-D	-4.13[NG]	4.88[G]	2.73[NG]	-1.24[G]
M06-2X	-3.75[NG]	4.67[NG]	1.84[NG]	-0.40[NG]
MP2	-6.36[NG]	4.70[NG]	-0.88[NG]	-1.23[G]
DMC/B3LYP	-5.3(2)[G]	4.89(2)[G]	1.6(4)[G]	-1.2(4)[G]
CCSD(T)	-5.24	4.89	0.94	-1.13

TABLE III. Summary of the abilities in describing each binding region at various levels of theory. NG/G in brackets stands for 'No Good'/'Good', respectively. Statistical errors in the DMC results are indicated in parentheses.

	B3LYP-GD3	MP2	CCSD(T)	DMC
$p(\alpha)/R_{\text{diag}}$	0.343/6.6	0.293/6.3	0.327/6.4	0.48(27)/6.5
$p(\beta)/R_{\text{diag}}$	0.243/6.7	0.248/6.3	0.245/6.5	0.21(7)/6.6
$p(\gamma)/R_{\text{diag}}$	0.243/6.6	0.248/6.1	0.245/6.3	0.21(7)/6.4
$p(\delta)/R_{\text{diag}}$	0.172/6.6	0.210/6.1	0.183/6.2	0.09(19)/6.4
\bar{R}_{tetra}	6.6	6.2	6.4	6.5(2)

TABLE IV. Comparisons of the equilibrium stability among four clustering configurations in Fig. 3, in terms of the thermal probability weight, $p \sim \exp(-\Delta E/kT)$. R_{diag} [Å] stands for the diagonal length for each tetramer, and \bar{R}_{tetra} [Å] is the thermal averaged diagonal length at $T = 298.15$ K.

second-order perturbative dispersion corrections (two-body term). [47] Both B97-D and B3LYP-GD2 give poor estimates of binding energies and lengths, but the former behaves better than the latter at long-range region, being appropriate for the estimation of Hamaker constants. This implies long-range behaviors also depend on original functionals, and atom-pairwise dispersion corrections do not necessarily lead to a correct description of 'molecule-pairwise' dispersion interactions, as in the B3LYP-GD2 case. It has been reported that DFT-D3 including atom-pairwise third-order perturbative dispersion corrections (three-body term) can remedy this kind of discrepancy in long-range as well as equilibrium behaviors at the DFT-D2 level of theory [48]. It is notable that the present B3LYP-GD3 binding curve is well improved in its long-range behavior to reproduce a correct decaying exponent. For the present CHS case, its correct molecule-pairwise dispersion behavior at long-range region requires both the second- and third-order perturbative dispersion corrections. Looking at the short-range region, on the other hand, we find that B97-D and M06-2X give a better description than B3LYP-GD3, getting closer to the DMC and CCSD(T) estimations. This suggests that B3LYP-GD3 includes too large Hartree-Fock exchange effects to be adequately canceled out by correlation effects. The above results can be summarized in Table III.

Our DMC and MP2 results are shown in Fig. 4 (b), compared with the reference CCSD(T), the typical SCF (B3LYP), and the best within DFT at equilibrium and long-range regions (B3LYP-GD3). As is well known, MP2 overbinds with deeper (shorter) binding energy (distance). [49] It may not be surprising to get the co-

incidence of asymptotic behaviors between MP2 and CCSD(T), because the present CCSD(T) is corrected by the CBS scheme taken from MP2 [50] (see Supporting Information). Three DMC curves were obtained starting from guiding functions generated by LDA, PBE, and B3LYP, respectively (see Supporting Information). They almost converged to the same binding curve, even starting from either B3LYP (worst in reproducing binding at SCF level) or LDA (too deep spurious overbinding at SCF level). Similar insensitivity to the choice of guiding functions has been also reported for a DNA stacking case, [28] implying that these DMC predictions are not seriously affected by the fixed-node approximation. Based on the variational principle with respect to nodal surfaces in DMC [51–53], we henceforth concentrate on the B3LYP guiding function only, because it gives the lowest total energy though the energy differences among the three binding curves are quite small. Note that this is consistent with a number of previous DMC studies [28, 54–57]

The present DMC is found to give almost the same results as CCSD(T). A remarkable difference between CCSD(T) and DMC is the binding energy at short range, $\Delta E(4.2)$ by $\sim 0.6(\pm 0.4)$ kcal/mol. The difference would be partly attributed to the dynamical correlation effect, which becomes more important at shorter binding length as well as exchange repulsions. Even under the fixed-node approximation, the dynamical correlation is expected to be well described, [17, 18, 23–31] and hence the present DMC curve is regarded as the best description of the binding of CHS.

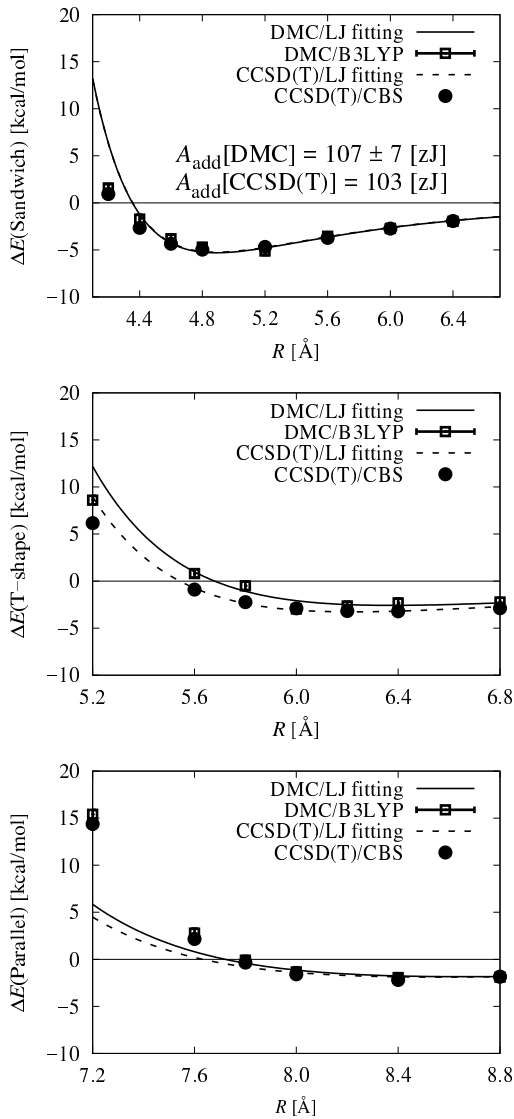


FIG. 2. DMC binding curves for three types of coalescence (Sandwich/T-shape/Parallel) compared with CCSD(T). For eye-guide, Lennard-Jones fitting is depicted for both DMC and CCSD(T), though for T-shape and Parallel, the fitting has a limited meaning because they do not behave like R^{-6} (see Appendix D for details)

Practicality: DMC vs. CCSD(T)

Fig. 5 shows the comparison between DMC and CCSD(T) with and without basis set (CBS) corrections. Even though CCSD(T) is known as the 'gold standard' among *ab initio* predictions, the practical use of CCSD(T) requires very careful handling of corrections, as described in Supporting Information, to get enough reliable predictions. [58] The correction itself is also un-

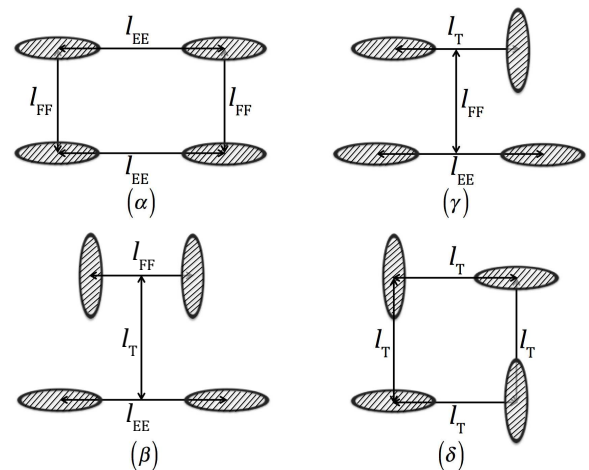


FIG. 3. Possible four-body clusterings formed from the two-body coalescences shown in Fig. 1. Hatched regions stand for the surfaces surrounded by the ring of cyclohexasilane molecule. l_{FF} , l_{T} , and l_{EE} correspond to the binding lengths with 'face-to-face', 'T-shape', and 'edge-to-edge' configuration, respectively.

der quite a limited approximation [50, 59] (see Eq. (1) in Supporting Information). These practical limitations are, in contrast, not the case in DMC because it is free from the basis set choice to the extent that only the nodal structure of the many-body wavefunction is fixed by the given basis set. In order to evaluate Hamaker constants of practically larger systems, therefore, DMC has the advantage over CCSD(T) with less sensitivity to basis sets.

CONCLUDING REMARKS

We considered a scheme using DMC-PES to evaluate Hamaker constants A for practical anisotropic molecules, and applied it to a cyclohexasilane (CHS) molecule used as an ink for printed electronics. The scheme should take into account two important factors for practical applications, namely the weak molecular interactions dominated by electron correlations (especially dispersion), and non-unique coalescing direction between anisotropic molecules. By making comparisons with the estimations by Lifschitz theory (A_{L}) on benzene, we clarified several possible origins to give systematic biases on A_{add} when it is estimated by PES with/without any averaging operations over anisotropy. The success of our scheme in the benzene case leads us to its application to CHS. In the application to CHS, our DMC results coincides fairly well with other correlation methods such as CCSD(T), MP2, and several DFT with exchange-correlation functionals for molecular interactions, like B3LYP-GD3. The evaluated binding curve can be re-

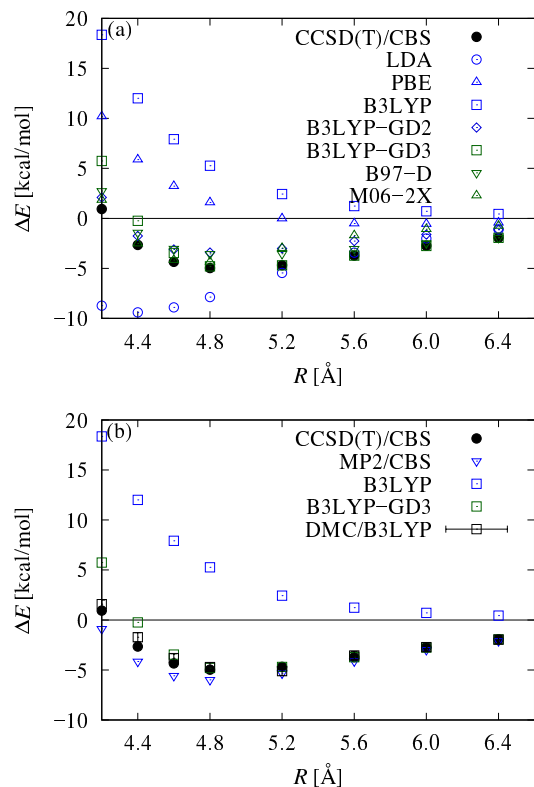


FIG. 4. Binding curves of Type-A (parallel) dimer coalescence evaluated by (a) DFT methods (LDA, PBE, B3LYP, B3LYP-GD2/GD3, B97-D, M06-2X) and (b) correlation methods (MP2, CCSD(T) and DMC/B3LYP) compared with selected DFTs. All the curves (except DMC) are corrected by BSSE and CBS (see Supporting Information for more details).

sonably validated by the experimentally observed density of the liquid solution via a scheme to relate its binding length and the mean inter-molecule distance. We find out that the parallel-wise coalescence of molecules gives the longest distant exponent for the interaction, being around 6.0. Several possible fitting schemes are applied to get A_{add} , and finally we estimate it around 105 ± 2 [zJ], with practically enough small statistical error. Though there is no experimental data available for a direct comparison, the present estimation is well supported from the trend of both Hamaker constants for similar kinds of molecules and of systematic difference between the predictions by the Lifshitz theory and by the asymptotic exponent estimations.

ASSOCIATED CONTENT

The BSSE and CBS corrections to the SCF and correlated methods and the time-step bias in DMC are discussed in more detail at Supporting Information. This material is available free of charge via the Internet at

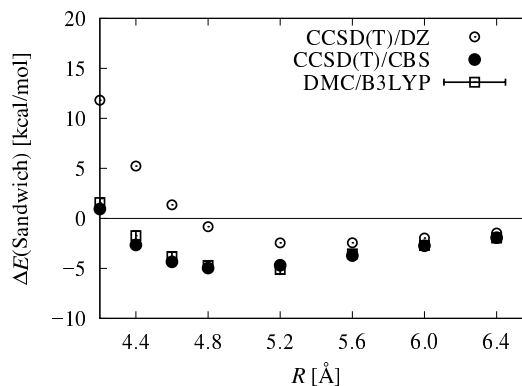


FIG. 5. Comparison of binding curves between DMC and BSSE-corrected CCSD(T) with the CBS/DZ basis set. 'CCSD(T)/DZ[CBS]' stands for the raw value without any corrections by DZ basis sets [CBS limit], while 'BSSE-CCSD(T)/DZ[CBS]' means that with BSSE corrections.

<http://pubs.acs.org>

ACKNOWLEDGMENTS

The authors thank Mr. M. Imamura for his preliminary calculations. K.H. is grateful for financial support from a KAKENHI grant (15K21023), a Grant-in-Aid for Scientific Research on Innovative Areas (16H06439), PRESTO and the Materials research by Information Integration Initiative (MI²I) project of the Support Program for Starting Up Innovation Hub from Japan Science and Technology Agency (JST). R.M. is grateful for financial support from MEXT-KAKENHI grants 26287063 and that from the Asahi glass Foundation. The computation in this work has been mostly done using the facilities of the Center for Information Science in JAIST.

APPENDIX

A. Computational Methods

The binding curves are evaluated by DMC, compared with CCSD(T), MP2, and several DFT calculations with various XC functionals. As a common choice, the fixed-node approximation [17, 18] was made to the DMC simulations (DMC), taking Slater-Jastrow wavefunctions as the guiding functions. The Slater determinants are composed of Kohn-Sham (KS) orbitals obtained using Gaussian09 [36] with Burkatzki-Filippi-Dolg (BFD) pseudo potentials (PP) [60] and its accompanying VTZ Gaussian basis sets. The BFD-PPs have been proved to give enough practical accuracies not only in DMC but also DFT on the applications such as a DNA stacking prob-

lem. [28]

Our Jastrow functions [61, 62] were those implemented in CASINO [17], consisting of one-, two-, and three-body contributions, denoted as χ -, u -, and F -terms, respectively. The χ -, u -, and F -terms include 16, 16, and 32 adjustable parameters, respectively. They were optimized by the variance minimization scheme [63, 64]. The electron-electron cusp condition [65] was imposed only on the u -term during the optimization procedure. For DMC statistical accumulations, we set the target population (the number of random walkers) to be 1,024 configurations in average and the time step to be $\delta t = 0.02$ in atomic unit. The time step bias [66] arising from this choice is discussed in Supporting Information. We took averages over 1.7×10^5 accumulation steps after the equilibration of 10^3 steps. We also used T -move scheme [53] for the locality approximation to the evaluation of PPs [51, 52] in DMC.

Only for Type-A, we benchmarked various DFT-SCF calculations for a comparison with DMC, seeing how the choice of the XC functionals affects the trial nodal structures in DMC. Our choice of XC functionals in DFT includes those recently designed for molecular interactions, B3LYP+GD2 [47]/GD3, [48] M06-2X, [67] and B97-D, [47] as well as LDA [68], PBE [69], B3LYP [70–72].

For a systematic comparison, we consistently used the same basis sets as DMC, VTZ basis sets provided in BFD-PP library [60]. For correlated methods (MP2 and CCSD(T)), however, the VTZ is too large to be accommodated in tractable memory capacities (512GB shared by 64 parallel cores in SGI Altix UV1000). To correct biases due to basis sets choices, we considered Complete Basis Set (CBS) methods [50, 59] with two different basis sets, and counterpoise methods for basis set superposition error (BSSE). [16, 43–45] Detailed discussions about these corrections are given in Supporting Information. All the DFT-SCF and correlated calculations were performed using Gaussian09. [36]

As demonstrated in Supporting Information, all the three functionals give almost the same binding energy and equilibrium distance, but B3LYP is found to give the best nodal surface in the sense of the variational principle. Hence we concentrated only on B3LYP orbitals for DMC for Type-B and -C.

B. Summary of formalisms of Hamaker constants

In most of practical cases, the Hamaker constants are estimated by the macroscopic frameworks based on Lifshitz theory [40] (let us denote the estimation by this frameworks as A_L). In the scheme, $A_{\text{add}} = \pi C_6 \rho^2$, several possibilities are available for C_6 evaluations, including those (i) by DOSD (dipole oscillator strength distribution) experiments, [73] (ii) by estimations by the

Casimir-Polder relation (CPR) [74] using *ab initio* evaluations of dynamical polarizabilities, [75, 76] and (iii) by the fitting of asymptotic behaviors in the molecular binding curves, or potential energy surfaces (PES), evaluated by *ab initio* calculations. [77] The Casimir-Polder formula for (ii) is given in hartree units as,

$$C_6 = \frac{3}{\pi} \int_0^\infty du \cdot \bar{\alpha}(iu)^2, \quad (2)$$

in an integral over the imaginary frequency, iu , of the orientation average of the polarization tensor, $\bar{\alpha}(iu) := (1/3)\text{Tr}[\alpha(iu)]$. $\bar{\alpha}$ can be evaluated by TDDFT (time-dependent DFT) within the linear response theory. [75, 76] Provided that the molecule has a unique absorption frequency (ionization energy), $\nu_I (= I/h)$, a further approximation with $\bar{\alpha}(iu) \approx \bar{\alpha}(0)\nu_I^2/(u^2 + \nu_I^2)$ substituted to (eq. (2)) leads to the London formula of the dispersion force [37],

$$C_6 = \frac{3}{4}\bar{\alpha}^2(0)I, \quad (3)$$

where $\bar{\alpha}(0)$ is the static polarizability.

C_6 for practical anisotropic molecules obviously depends on the orientation of coalescence, such as T-shape, parallel, sandwich, *etc.* Plausible averaging is required over the possible orientations to get A_{add} , which is the main subject of the present study. This would be a reason that A_L is used much rather than A_{add} because in the former the non-additivity as well as the anisotropy are effectively taken into account by using macroscopically averaged quantities. In (i) and (ii), the macroscopic/observed quantities used in the formula would be regarded as the effective consideration of such averaging to give $\langle C_6 \rangle$, as we used in Table V. For most of the practical cases, the Hamaker constants are evaluated not by A_{add} but by A_L , a macroscopic framework based on Dzyaloshinskii-Lifshitz-Pitaevskii (DLP) theory, in which the Hamaker constant is expressed as an infinite series of an expansion. Truncation upto the second term gives a practical approximation, known as Ninhan-Parsegian formula [78, 79],

$$A_L = \frac{3}{4}kT \left(\frac{\epsilon - 1}{\epsilon + 1} \right)^2 + \frac{3h\nu_e}{16\sqrt{2}} \cdot \frac{(n^2 - 1)^2}{(n^2 + 1)^{3/2}}, \quad (4)$$

and its truncation error is estimated to be around 5%. [3] The Hamaker constant can then be evaluated using macroscopic quantities of the bulk, *i.e.*, dielectric constant ϵ , and the refractive index n (k and T are the Boltzmann constant and absolute temperature, respectively, while h and ν are the Planck constant and the frequency of the primary electronic excitation in ultra-violet range). Unlike A_{add} , the macroscopic A_L can avoid the additive assumptions, namely the macroscopic quantities effectively take into account the non-additivity as well as the anisotropy.

C. Comparison of different predictions of A

For the side-way manner of the validation of A predicted for CHS, we would like to know if there is a systematic bias between A_{add} and other macroscopic A_{L} . For this purpose, we take benzene as a representative tiny benchmark. In this case, there are many references to C_6 and A_{L} available in literature [3, 73, 75–77], by which we can survey the possible relation between A_{add} and A_{L} to get a plausible validation for the estimate of realistic Hamaker constants $A_{\text{add}}(C_6)$ evaluated from *ab initio* PES calculations. Even for this simple molecule, there has been little investigations relating it to A_{add} for practical molecules, though it is straightforward. This might be attributed to the difficulty of the averaging over anisotropic configurations of coalescence.

Table V summarizes the Hamaker constants estimated by several approaches explained in Appendix B. No.2-6 in Table V are obtained using C_6 evaluated by London’s theory, CPR, and DOSD, which can be regarded as an equivalent averaging over orientations to get a representative isotropic value, $\langle C_6 \rangle^{\text{iso}}$. For London’s theory (No.2/3), the closer values to A_{L} (No. 1) might be accidental. These should be comparable rather to No.4/5 but turned out to be underestimated by around 40%. The underestimation can be explained because, as we mentioned, the London theory only picks up single absorption frequency, ignoring other contributions which are all positive. No.4-6 are consistent with each other being around 75 [zJ], but overestimating when we take A_{L} as the reliable reference for the perfect averaging about the anisotropy and non-additivity. The importance of the anisotropy can be seen in No.7-9, where C_6 are evaluated only by PES for a coalescence configuration, such as Sandwich or T-shape. We see that different methods for PES give consistent results with each other for the same configuration (No.7 and No.8), while the same method gives the different estimation for different configurations (No.8 and No.9).

SAPT evaluations, No.10 and No.11, give some confidence about the effective isotropic averaging for No.4-6 and the importance to consider the anisotropy for the A_{L} value. In SAPT, the dispersion interaction is evaluated in the form,

$$E_{\text{disp}} \sim \frac{1}{R^6} \cdot \sum_{l_A, k_A, l_B, k_B, l} C_6[l_A, k_A, l_B, k_B, l] \cdot w_6[l_A, k_A, l_B, k_B, l](\omega_A, \omega_B, \Omega), \quad (5)$$

as the summation over the possible anisotropic configurations labelled by the rank of tensor $\{l_A, k_A, l_B, k_B, l\}$ with each weight w_6 . $\{\omega_A, \omega_B, \Omega\}$ denote the Euler angles between molecules A and B, and the solid angle between the molecules, respectively. No.10 is evaluated from the isotropic contribution, $C_6[0, 0, 0, 0, 0] = 1726$, and consistent with No.4-6 as expected. We

can also obtain the anisotropic contributions from the supplemental information of the paper [77], $C[0, 0, 2, 0, 2] = C[2, 0, 0, 0, 2] = -552$, $C[2, 0, 2, 0, 0] = 17$, $C[2, 0, 2, 0, 2] = 45$, $C[2, 0, 2, 0, 4] = 482$, to estimate No.11. To avoid the complicated averaging operations with serious weightings, we simply takes the arithmetic mean for isotropic and anisotropic contribution, and get $\langle C_6 \rangle^{\text{iso+aniso}}$ quite closer to A_{L} in No.1.

No.12/13 give the estimation by a single configuration, parallel-displacement (ParaDisp), which is identified as the most stable binding. [80] The estimation is made from the DMC data by Azadi *et al.*, [81] from which we fit C_6 using log plots (No.12) or 6-12 Lennard-Jones (LJ) potential (No.13) as shown in Fig. 6. Since we are interested in the long-range asymptotic behavior $\sim R^{-6}$, we did not take the original spline-like fitting function used in the paper, [81] which is used to describe the whole PES shape being different from the present purpose. We note for the log plot that the larger errorbar is a sort of inevitable consequence of log-plot for long-range exponents: [6] For a fixed magnitude of statistical errors over the range of distance R , any decreasing dependence on a log-plot gives inevitably enlarged errorbars as R increases (the resolution of the vertical axis gets enlarged downward by *definition*). In the present case, the statistical noise has been well suppressed less than 0.02 kcal/mol, and further reduction of the errorbar in A is not practical. In LJ fitting, on the other hand, enough practical reduction of the errorbar has been achieved. The estimation of the fitting actually depends on the choice of the details of fitting functions, and data range of the fitting, for which we have chose it carefully with some validation as shown in Appendix D. Despite a single configuration, the fitting for the parallel-displacement configuration, No.12/13, coincides well with A_{L} . This implies that the most stable binding configuration (parallel displacement in this case) is almost dominant and other possible configurations can be ignored for A .

D. Fitting scheme for C_6

Several different fitting schemes are possible to extract C_6 from PES, in principle, such as log-fit ($C_6^{\text{stable;LOG}}$), LJ-fit ($C_6^{\text{stable;LJ}}$), and the power-fit for the correlation contribution ($C_6^{\text{stable;Corr}}$). Table VI summarizes the fitting results of benzene using various kinds of fitting functions and the choices of data range to be fit. While every fitting seems to work fairly well as shown in Fig. 7, the estimations of A significantly depend on the arbitrary choice. We tried 6-12 LJ, 6-9 LJ, 6-exponential potential (6-exp) [82], and pairwise polynomial fitting function. [81] The choice of the fitting range is about whether we include the data at repulsive region (at $R = 3.0$) or not. Only for 6-exp we could not get reasonable convergence without the data point at $R = 3.0$ to increase the

Label	Scheme/Theory/Method	$C_6/10^3$ [au]	A [zJ]
1/ A_L	Exp/DLP	NA	50 ± 2^a
2/ $A_{\text{add}}(\langle C_6^{\text{London}} \rangle_{\text{iso}})$	London/HF	0.925 ^b	42
3/ $A_{\text{add}}(\langle C_6^{\text{London}} \rangle_{\text{iso}})$	London/B3LYP	1.105 ^c	48
4/ $A_{\text{add}}(\langle C_6^{\text{CPR}} \rangle_{\text{iso}})$	CPR/TDHF	1.737 ^d	75
5/ $A_{\text{add}}(\langle C_6^{\text{CPR}} \rangle_{\text{iso}})$	CPR/TDDFT	1.773 ^e	77
6/ $A_{\text{add}}(\langle C_6^{\text{DOSD}} \rangle_{\text{iso}})$	Exp/DOSD	1.723 ^f	74
7/ $A_{\text{add}}(C_6^{\text{PES}})$ (Sandwich)	PES/MP2	0.59 ^g	25
8/ $A_{\text{add}}(C_6^{\text{PES}})$ (Sandwich)	PES/CCSD(T)	0.602 ^h	26
9/ $A_{\text{add}}(C_6^{\text{PES}})$ (T-shape)	PES/CCSD(T)	3.911 ⁱ	169
10/ $A_{\text{add}}(\langle C_6^{\text{PES}} \rangle_{\text{iso}})$	PES/DFT-SAPT	1.726 ^j	74
11/ $A_{\text{add}}(\langle C_6^{\text{PES}} \rangle_{\text{iso+aniso}})$	PES/DFT-SAPT	1.165 ^k	50
12/ $A_{\text{add}}(C_6^{\text{PES}})$ (ParaDisp)	PES/DMC/log	1.25 ± 0.27^l	54 ± 12
13/ $A_{\text{add}}(C_6^{\text{PES}})$ (ParaDisp)	PES/DMC/LJ	1.19 ± 0.10^m	51 ± 4

TABLE V. Comparisons of Hamaker constants A of Benzene estimated by different schemes. The bracket, $\langle \dots \rangle$, means spatial averaging (see text for details).

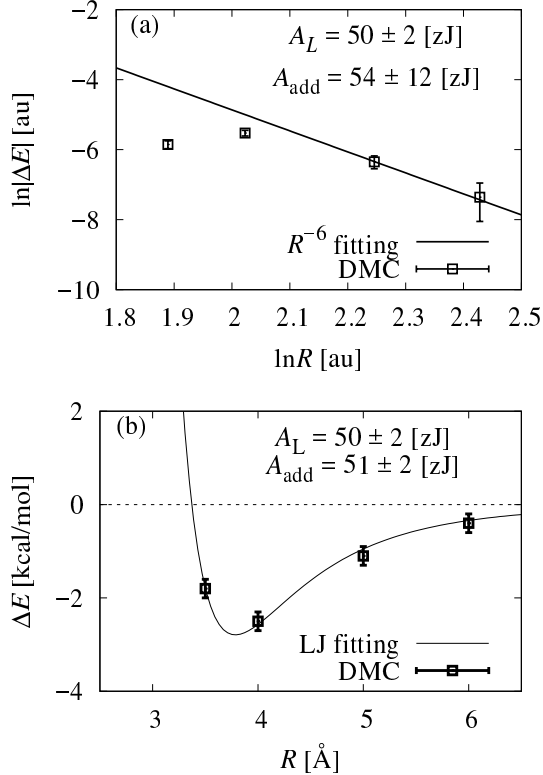


FIG. 6. DMC binding curves of benzene dimer: (a) logarithmic plot fitted by asymptotic R^{-6} behavior and (b) Lennard-Jones fitting.

data points for such a strong non-linear fitting. For the polynomial, we could not extract C_6 for the asymptotic R^{-6} behavior as we mentioned in the previous paragraph, but we can use it to get a reliable reference for the binding energy ΔE and bonding length R_e , as it is the most precise function for the whole fitting purpose as described in the paper. [81] Taking those reference for ΔE and R_e ,

we see that excluding the repulsion point, $R = 3.0$, from LJ fitting gives better estimations. Though the log-fitting result (No.12) in Table V has the large errorbar, the value is reliable to some extent in the aspect of the asymptotic behavior, from which 6-9 LJ (3.5 ~ 6.0) gives larger deviation. Based on these facts, we finally take 6-12 LJ (3.5 ~ 6.0) to provide the value (No.11) in Table V.

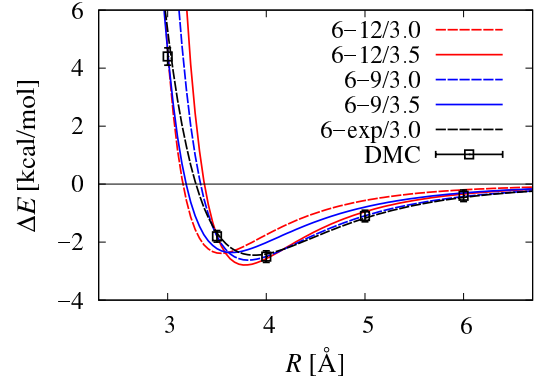


FIG. 7. Comparison between different fitting schemes of DMC binding curves (benzene dimer with parallel-displacement (PD) configuration) using 6-12 LJ (Lennard-Jones), 6-9 LJ, and 6-exp with different fitting ranges (e.g., '6-12/3.0' means the range starting from $R=3.0$ [Å]).

For CHS, the results using different fitting schemes were tabulated in Table II of main text. We start with the log-fit ($C_6^{\text{stable};\text{LOG}}$). To obtain plausible estimates of $C_6^{\text{stable};\text{LOG}}$, it is essential to choose their fitting region R_f at long-range. We focus on the relation that by definition the binding energy can be decomposed as the sum of Hartree-Fock (HF) and correlation contributions: $\Delta E(R) = \Delta E_{\text{HF}}(R) + \Delta E_{\text{corr}}(R)$ [83]. Since $\Delta E_{\text{HF}}(R)$ (exponentially) decays much faster than $\Delta E_{\text{corr}}(R)$ (polynomially) at large R , the asymptotic behavior is dominated by $\Delta E_{\text{corr}}(R)$. Thus, we choose R_f

Functions	Range	ΔE [kcal/mol]	R_e [Å]	A_{add} [zJ]
6-12 LJ	3.0 ~ 6.0	-2.4 ± 0.2	3.54 ± 0.01	29 ± 2
6-12 LJ	3.5 ~ 6.0	-2.8 ± 0.2	3.78 ± 0.02	51 ± 4
6-9 LJ	3.0 ~ 6.0	-2.4 ± 0.2	3.64 ± 0.01	52 ± 3
6-9 LJ	3.5 ~ 6.0	-2.6 ± 0.2	3.81 ± 0.03	76 ± 7
6-exp	3.0 ~ 6.0	-2.5	3.88	70 ± 11
Pairwise Poly. [81]	3.0 ~ 6.0	-2.7 ± 0.3	3.8 ± 0.3	NA
CCSD(T) reference ^a	Configuration	ΔE	R_e	
	PD (most stable)	-2.78	3.87	
	T-shape	-2.74	5.01	
	Sandwich	-1.81	6.09	

TABLE VI. Dependences of estimated binding energies (ΔE), binding lengths (R_e), and Hamaker constants (A_{add}) on the choices of fitting functions and fitting ranges. Reference values for ΔE and R_e by CCSD(T) are also shown.

such that $R \in R_f$ satisfies $|E_{\text{HF}}(R)/E_{\text{corr}}(R)| < (1/10)$. Asymptotic exponents can be extracted from the log-plots, as shown in Fig. 8. The best fits of the exponents in DMC [CCSD(T)] give -5.6 ± 5.8 [-5.9], -4.2 ± 5.9 [-7.3], and -7.2 ± 7.2 [-8.7] for Type-A, B, and C, respectively. Supported by the CCSD(T) estimations, we can somehow identify that Type-A dominates the wettability with the longest-ranged exponent that is almost close to the $\sim C_6/R^6$ dependence. For Type-A, we can then identify the C_6 constant from the fitting with exponent fixed to be 6.0. To sum up, only the stable configuration contributes to $\sim 1/R^6$ asymptotic behavior while the other give different exponents. Note that this 'less contributions to A ' from other meta-stable configurations is quite in contrast to the case for the molecular density estimation, for which only the stable binding configuration cannot reproduce the proper density, as describe in Appendix E.

As was explained in the benzene case, the log-fits are inevitably accompanied by the larger statistical errorbars. If we aimed to reduce the errorbar by one more digit, 100 times more statistical accumulation would be necessary. This computation corresponds to 2.2×10^6 core-hours (half a year CPU time on 512 cores parallel, provided that we can keep on using it without any queue), and hence is impractical.

The larger errorbars in the log-fitting are much improved by using the other fitting schemes: The present study employed the 6-12 LJ fitting (Fig. 2 of main text) using

$$U(R) = -\frac{C_6}{R^6} + \frac{C_{12}}{R^{12}}. \quad (6)$$

and the correlation fitting (Fig. 9) based on a power expansion, [37, 38]

$$\Delta E_{\text{corr}}(R) \sim -\frac{C_6}{R^6}, \quad (7)$$

to extract C_6 from PES. As was discussed in the benzene case, the estimation depends on the data fitting range, and then some plausible choice is required. Table VII

compares the choices especially about whether the range includes repulsive region ($R < 4.4$) or not. To get the best choice, we adopted a figure of merit,

$$f = \sum_{j=1} \frac{(\Delta E(R_j) - U(R_j))^2}{\sigma(R_j)^2}, \quad (8)$$

as defined using the deviation of $\Delta E(R_j)$ from the fitting, weighted by the statistical error $\sigma(R_j)$ in DMC [which is set to be unity for CCSD(T)]. For the 6-12 LJ fitting, we chose the estimations achieving minimum f , those with the range $R = 4.6 \sim 6.4\text{Å}$, as finally tabulated in Table II.

For the correlation fitting, the final choices in Table II of main text are also those which achieve minimum f in Table VII, as we did for the 6-12LJ case. The correlation fitting, if tractable, would be more plausible in the following sense: (i) Its theoretical background is sound (perturbation theory on electron correlation at long-range). (ii) Base on the theory, it is obvious to exclude the repulsive (short-range) region from the fitting region. (iii) Hence there is no ambiguity about the model function to describe the repulsive region such as 6-12/6-9 LJ or 6-exp. (iv) Since ΔE_{corr} increases monotonically, a better and more (numerically) stable fitting can be expected.

E. Binding length and Density

A PES gives a binding length R_e , which would have some relation to the experimental molecular density. Once some reliable relation was established, we can use it to validate the binding curve calculation. The relation is however not so clearcut as we describe below. The experimental density of the benzene liquid [84] gives an estimate of mean intermolecular distance as $R_\rho \sim 5.3\text{Å}$, being far larger than R_e in the most stable binding by 26%. This is quite in contrast to the case of A where only the most stable configuration seems dominant. The simplest idea is to take into account the contributions not only from the most stable parallel displacement ($\Delta E = -2.78\text{kcal/mol}$; $R_e = 3.87\text{Å}$), but also other

Method	$U(R)$	R_f	ΔE	R_e	A_{add}	f
DMC	6-12 LJ	4.2 ~ 6.4	-4.9 ± 0.2	4.74 ± 0.01	85 ± 4	1.198
	6-12 LJ	4.4 ~ 6.4	-5.2 ± 0.2	4.79 ± 0.01	100 ± 5	0.113
	6-12 LJ	4.6 ~ 6.4	-5.3 ± 0.2	4.89 ± 0.02	107 ± 7	0.033
	6-12 LJ	4.8 ~ 6.4	-5.2 ± 0.2	4.96 ± 0.03	112 ± 9	0.206
	Corr.	4.2 ~ 6.4			103 ± 1	0.022
	Corr.	4.4 ~ 6.4			105 ± 2	0.005
	Corr.	4.6 ~ 6.4			108 ± 2	0.020
	Corr.	4.8 ~ 6.4			110 ± 5	0.062
CCSD(T)	6-12 LJ	4.2 ~ 6.4	-5.10	4.76	86	0.027
	6-12 LJ	4.4 ~ 6.4	-5.27	4.82	95	0.004
	6-12 LJ	4.6 ~ 6.4	-5.24	4.89	103	0.002
	6-12 LJ	4.8 ~ 6.4	-5.12	4.94	107	0.006
	Corr.	4.2 ~ 6.4			106	0.018
	Corr.	4.4 ~ 6.4			108	0.034
	Corr.	4.6 ~ 6.4			110	0.053
	Corr.	4.8 ~ 6.4			110	0.050

TABLE VII. Dependence of the Hamaker constant A_{add} on types of fitting functions $U(R)$ fitted within ranges U_f for DMC and CCSD(T). The best choice of ranges were chosen such that values of figure of merit f (see text for definition) achieves minimum. For the 6-12 LJ fitting, binding energies ΔE and binding lengths R_e were also listed.

meta-stable ones, T-shape (-2.74kcal/mol ; 5.01\AA), and Sandwich (-1.81kcal/mol ; 6.09\AA). Only the most unstable configuration (Sandwich) has a longer binding length of $R = 6.09\text{\AA}$, and the thermal averaging with the weight $p \sim \exp(-\Delta E/kT)$ at $T = 298.15\text{K}$ gives $\bar{R}_{\text{dim}} = 4.5\text{\AA}$, being 15% underestimation.

As one of the possible origin for the discrepancy, we might consider the intra-molecular relaxation, but it is unlikely to account for it: the relaxation will bring energy gains at shorter binding lengths when the molecule deforms by the binding interaction, and hence make the binding length shorter, being further away from R_ρ .

Further consideration makes us realize that we took into account only two-body coalescences to argue the mean separation. When we consider further four-body clusterings possibly occurring in realistic liquids, we notice that the mean separation seems to be dominated rather by the longest binding length among the possible coalescence: The mean value can roughly be estimated by the 'diagonal lengths' of four-body trapezoids, as shown in Fig. 3 of main text. Taking the center of gravity of each molecule as the vertices of trapezoids, the 'diagonal lengths' can be defined as the square root of the area of a trapezoid, which is dominated rather by the longest distant binding pair. Estimating the possibility weight for each trapezoid as the Boltzmann weight with the sum of the binding pair energies, ΔE , then the thermal averaging over the 'diagonal lengths', $l_{\text{FF}} = 3.9\text{\AA}$ (face-to-face), $l_{\text{T}} = 5.1\text{\AA}$ (T-shape), and $l_{\text{EE}} = 6.0\text{\AA}$ [85] (edge-to-edge), gives an improved estimate of $\bar{R}_{\text{tetra}} = 5.0\text{\AA}$, getting closer to the experimental estimation of $R_\rho \sim 5.3\text{\AA}$.

The discrepancy still left would further be reduced by considering the higher order clustering as well as the atomic vibration at finite temperature, [86] but the present simple idea about four-body trapezoids seems

quite successful.

The above scheme also works for CHS, as shown in the main text (See "Validation of equilibrium properties"). For CHS, we can directly estimate the binding energy, ΔE , and the equilibrium binding length, R_e , by fitting the data using an equivalent form of Eq. (6),

$$U(R) = \Delta E \left[2 \left(\frac{R_e}{R} \right)^6 - \left(\frac{R_e}{R} \right)^{12} \right], \quad (9)$$

as summarized in Table III of main text. Note that we can also estimate ΔE and R_{eq} 'after' the fitting (C_6, C_{12}) first by Eq. (6) in Appendix D, but this is not a good idea for DMC because the error propagation for statistical noises during the further transformation to ΔE and R_e loses the accuracy of estimates. Fitting curves well describe the dependence around equilibrium lengths, as shown in Fig. 2 of main text. For Type-B and C with shorter-ranged exponents, it is not rigorously validated to use the LJ potential because its functional form assumes the $1/R^6$ asymptotic behavior. We use it, however, under such a limited reason just to get possible estimates of ΔE and R_e even for Type-B and C, as given in Table I of main text.

We obtained $R_\rho = 6.8\text{\AA}$ from experimental values of the molecular weight (180.61 g/mol) and density (0.97 g/cm^3 at $T = 298.15\text{K}$), which fairly reasonably drops within the binding lengths of Type-A to C. Similar to the benzene case, the simple thermal averaging over the three configurations by the factor, $p \sim \exp(-\Delta E/kT)$ at $T = 298.15\text{K}$ underestimates $\bar{R}_{\text{dim}} \sim 4.9\text{\AA}$, compared with R_ρ . An alternative averaging over the 'diagonal lengths' of four-body trapezoids, as shown in Fig. 3, gives an improved estimate, \bar{R}_{tetra} , getting closer to the experimental estimation, as shown in Table IV of main text.

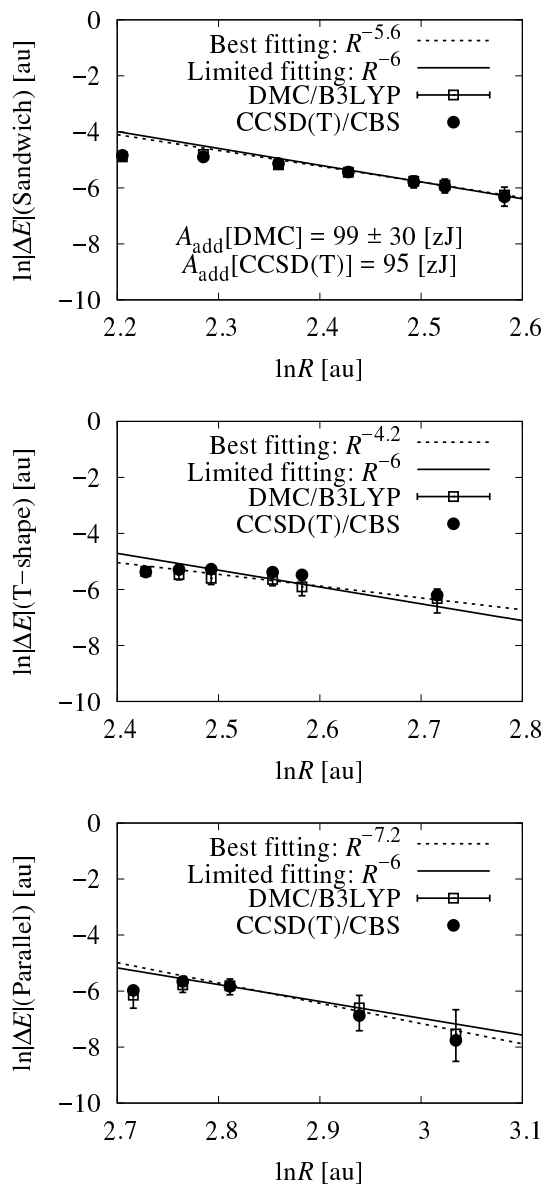


FIG. 8. Asymptotic behaviors of binding curves evaluated by DMC and CCSD(T), as given in logarithmic plots fitted by two different lines, 'Best' and 'Limited'. In the former fitting, the exponent is fitted to get the best fitting while in the latter it is fixed to be assumed R^{-6} behavior.

* kenta_hongo@mac.com

† National Institute for Materials Science (NIMS), 1-2-1 Sengen, Tsukuba, Ibaraki 305-0047, Japan; PRESTO, JST, 4-1-8 Honcho, Kawaguchi, Saitama 332-0012, Japan
 [1] H. Hamaker, *Physica* **4**, 1058 (1956).
 [2] D. Bonn, J. Eggers, J. Indekeu, J. Meunier, and E. Rolley, *Rev. Mod. Phys.* **81**, 739 (2009).
 [3] J. N. Israelachvili, *Intermolecular and Surface Forces (Third Edition)*, third edition ed., tagkey2011iii (Aca-

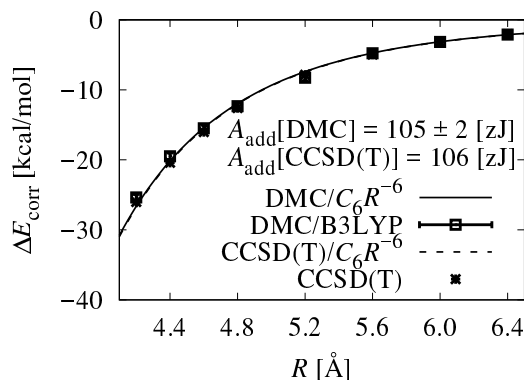


FIG. 9. Correlation energy contributions to binding energies evaluated by DMC and CCSD(T).

demic Press, San Diego, 2011).

- [4] D. Levy and M. Zayat, eds., *The Sol-Gel Handbook: Synthesis, Characterization and Applications, 3-Volume Set* (Wiley, 2015).
 [5] T. Shimoda, Y. Matsuki, M. Furusawa, T. Aoki, I. Yudasaka, H. Tanaka, H. Iwasawa, D. Wang, M. Miyasaka, and Y. Takeuchi, *Nature* **440**, 783 (2006).
 [6] A. J. Misquitta, R. Maezono, N. D. Drummond, A. J. Stone, and R. J. Needs, *Phys. Rev. B* **89**, 045140 (2014).
 [7] A. J. Stone, ed., *The Theory of Intermolecular Forces* (Oxford University Press, Oxford, U.K., 1997).
 [8] I. G. Kaplan, ed., *Intermolecular Interactions* (J. Wiley & Sons, Chichester, U.K., 2006).
 [9] P. H. Lau, K. Takei, C. Wang, Y. Ju, J. Kim, Z. Yu, T. Takahashi, G. Cho, and A. Javey, *Nano Lett.* **13**, 3864 (2013), <http://dx.doi.org/10.1021/nl401934a>.
 [10] S. Inoue, T. Ariga, S. Matsumoto, M. Onoue, T. Miyasako, E. Tokumitsu, N. Chinone, Y. Cho, and T. Shimoda, *J. Appl. Phys.* **116**, 154103 (2014).
 [11] Y. Nakamura, A. Carlson, G. Amberg, and J. Shiomi, *Phys. Rev. E* **88**, 033010 (2013).
 [12] H. Matsui, Y. Noda, and T. Hasegawa, *Langmuir* **28**, 15450 (2012), <http://dx.doi.org/10.1021/la303717n>.
 [13] A. J. Cohen, P. Mori-Sánchez, and W. Yang, *Chem. Rev.* **112**, 289 (2012), <http://dx.doi.org/10.1021/cr200107z>.
 [14] K. S. Kim, S. Karthikeyan, and N. J. Singh, *J. Chem. Theory Comput.* **7**, 3471 (2011), <http://dx.doi.org/10.1021/ct200586g>.
 [15] P. Hobza and K. Muller-Dethlefs, *Non-Covalent Interactions*, RSC Theoretical and Computational Chemistry Series (The Royal Society of Chemistry, 2009) pp. P001–P226.
 [16] T. Helgaker, P. Jørgensen, and P. Olsen, *Molecular Electronic-Structure Theory* (Wiley, Chichester, U.K., 2000).
 [17] R. J. Needs, M. D. Towler, N. D. Drummond, and P. L. Ríos, *J. Phys.: Condens. Matter* **22**, 023201 (2010).
 [18] B. M. Austin, D. Y. Zubarev, and W. A. Lester, *Chem. Rev.* **112**, 263 (2012), <http://pubs.acs.org/doi/pdf/10.1021/cr2001564>.
 [19] Y. Uejima, T. Terashima, and R. Maezono, *J. Comput. Chem.* **32**, 2264 (2011).
 [20] Y. Uejima and R. Maezono, *J. Comput. Chem.* **34**, 83

- (2013).
- [21] K. Hongo, Y. Kawazoe, and H. Yasuhara, *MATERIALS TRANSACTIONS* **47**, 2612 (2006).
- [22] K. Hongo, Y. Kawazoe, and H. Yasuhara, *International Journal of Quantum Chemistry* **107**, 1459 (2007).
- [23] M. Korth, A. Luchow, and S. Grimme, *J. Phys. Chem. A* **112**, 2104 (2008), <http://pubs.acs.org/doi/pdf/10.1021/jp077592t>.
- [24] L. Horváthová, M. Dubecký, L. Mitas, and I. Štich, *J. Chem. Theory Comput.* **9**, 390 (2013), <http://pubs.acs.org/doi/pdf/10.1021/ct300887t>.
- [25] L. Horváthová, R. Derian, L. Mitas, and I. Štich, *Phys. Rev. B* **90**, 115414 (2014).
- [26] M. Dubecký, P. Jurečka, R. Derian, P. Hobza, M. Otyepka, and L. Mitas, *J. Chem. Theory Comput.* **9**, 4287 (2013), <http://pubs.acs.org/doi/pdf/10.1021/ct4006739>.
- [27] M. Dubecký, R. Derian, P. Jurečka, L. Mitas, P. Hobza, and M. Otyepka, *Phys. Chem. Chem. Phys.* **16**, 20915 (2014).
- [28] K. Hongo, N. T. Cuong, and R. Maezono, *J. Chem. Theory Comput.* **9**, 1081 (2013), <http://pubs.acs.org/doi/pdf/10.1021/ct301065f>.
- [29] K. Hongo, M. A. Watson, R. S. Sánchez-Carrera, T. Iitaka, and A. Aspuru-Guzik, *J. Phys. Chem. Lett.* **1**, 1789 (2010), <http://pubs.acs.org/doi/pdf/10.1021/jz100418p>.
- [30] M. A. Watson, K. Hongo, T. Iitaka, and A. Aspuru-Guzik, “A benchmark quantum monte carlo study of molecular crystal polymorphism: A challenging case for density-functional theory,” in *Advances in Quantum Monte Carlo*, Chap. 10, pp. 101–117, <http://pubs.acs.org/doi/pdf/10.1021/bk-2012-1094.ch009>.
- [31] K. Hongo, M. A. Watson, T. Iitaka, A. Aspuru-Guzik, and R. Maezono, *J. Chem. Theory Comput.* **11**, 907 (2015), <http://dx.doi.org/10.1021/ct500401p>.
- [32] K. Hongo and R. Maezono, “Practical diffusion monte carlo simulations for large noncovalent systems,” in *Recent Progress in Quantum Monte Carlo*, Chap. 9, pp. 127–143, <http://pubs.acs.org/doi/pdf/10.1021/bk-2016-1234.ch009>.
- [33] M. Dubecký, L. Mitas, and P. Jurečka, *Chemical Reviews* **116**, 5188 (2016), PMID: 27081724, <http://dx.doi.org/10.1021/acs.chemrev.5b00577>.
- [34] M. K. Leong, V. S. Mastryukov, and J. E. Boggs, *J. Phys. Chem.* **98**, 6961 (1994), <http://dx.doi.org/10.1021/j100079a013>.
- [35] B. L. Kormos, C. J. Cramer, and W. L. Gladfelter, *J. Phys. Chem. A* **110**, 494 (2006), <http://dx.doi.org/10.1021/jp051885+>.
- [36] M. J. Frisch, G. W. Trucks, H. B. Schlegel, G. E. Scuseria, M. A. Robb, J. R. Cheeseman, G. Scalmani, V. Barone, B. Mennucci, G. A. Petersson, H. Nakatsuji, M. Caricato, X. Li, H. P. Hratchian, A. F. Izmaylov, J. Bloino, G. Zheng, J. L. Sonnenberg, M. Hada, M. Ehara, K. Toyota, R. Fukuda, J. Hasegawa, M. Ishida, T. Nakajima, Y. Honda, O. Kitao, H. Nakai, T. Vreven, J. A. Montgomery, Jr., J. E. Peralta, F. Ogliaro, M. Bearpark, J. J. Heyd, E. Brothers, K. N. Kudin, V. N. Staroverov, R. Kobayashi, J. Normand, K. Raghavachari, A. Rendell, J. C. Burant, S. S. Iyengar, J. Tomasi, M. Cossi, N. Rega, J. M. Millam, M. Klene, J. E. Knox, J. B. Cross, V. Bakken, C. Adamo, J. Jaramillo, R. Gomperts,
- R. E. Stratmann, O. Yazyev, A. J. Austin, R. Cammi, C. Pomelli, J. W. Ochterski, R. L. Martin, K. Morokuma, V. G. Zakrzewski, G. A. Voth, P. Salvador, J. J. Dannenberg, S. Dapprich, A. D. Daniels, Ö. Farkas, J. B. Foresman, J. V. Ortiz, J. Cioslowski, and D. J. Fox, “Gaussian 09 revision d.01,” Gaussian Inc. Wallingford CT 2009.
- [37] F. London, *Trans. Faraday Soc.* **33**, 8b (1937).
- [38] S. Grimme, A. Hansen, J. G. Brandenburg, and C. Bannwarth, *Chem. Rev.* **116**, 5105 (2016), <http://dx.doi.org/10.1021/acs.chemrev.5b00533>.
- [39] S.-B. Choi, B.-K. Kim, P. Boudjouk, and D. G. Grier, *Journal of the American Chemical Society* **123**, 8117 (2001), <http://dx.doi.org/10.1021/ja002831a>.
- [40] E. Lifshitz, *Soviet Phys. JETP* **2**, 73 (1956).
- [41] B. Silvana and A. Castro, *Nature* **78**, 035333:1 (2008).
- [42] N. N. Greenwood and A. Earnshaw, *Chemistry of the Elements (Second Edition)* (Butterworth-Heinemann, 1997).
- [43] S. Boys and F. Bernardi, *Mol. Phys.* **19**, 553 (1970), <http://dx.doi.org/10.1080/00268977000101561>.
- [44] F. B. van Duijneveldt, J. G. C. M. van Duijneveldt-van de Rijdt, and J. H. van Lenthe, *Chem. Rev.* **94**, 1873 (1994), <http://dx.doi.org/10.1021/cr00031a007>.
- [45] S. Simon, M. Duran, and J. J. Dannenberg, *J. Chem. Phys.* **105**, 11024 (1996).
- [46] A. Tkatchenko and O. A. von Lilienfeld, *Phys. Rev. B* **78**, 045116 (2008).
- [47] S. Grimme, *J. Comput. Chem.* **27**, 1787 (2006).
- [48] S. Grimme, J. Antony, S. Ehrlich, and H. Krieg, *J. Chem. Phys.* **132**, 154104 (2010).
- [49] K. E. Riley, J. A. Platts, J. Řezáč, P. Hobza, and J. G. Hill, *J. Phys. Chem. A* **116**, 4159 (2012), <http://dx.doi.org/10.1021/jp211997b>.
- [50] M. O. Sinnokrot and C. D. Sherrill, *J. Phys. Chem. A* **108**, 10200 (2004), <http://dx.doi.org/10.1021/jp0469517>.
- [51] P. J. Reynolds, D. M. Ceperley, B. J. Alder, and W. A. Lester, *J. Chem. Phys.* **77**, 5593 (1982).
- [52] L. Mitáš, E. L. Shirley, and D. M. Ceperley, *J. Chem. Phys.* **95**, 3467 (1991).
- [53] M. Casula, *Phys. Rev. B* **74**, 161102 (2006).
- [54] K. Hongo and R. Maezono, *International Journal of Quantum Chemistry* **112**, 1243 (2012).
- [55] J. Kolorenč, S. Hu, and L. Mitas, *Phys. Rev. B* **82**, 115108 (2010).
- [56] M. C. Per, K. A. Walker, and S. P. Russo, *J. Chem. Theory Comput.* **8**, 2255 (2012), <http://dx.doi.org/10.1021/ct200828s>.
- [57] K. Hongo and R. Maezono, “A quantum monte carlo study of the ground state chromium dimer,” in *Advances in Quantum Monte Carlo*, Chap. 8, pp. 91–99, <http://pubs.acs.org/doi/pdf/10.1021/bk-2012-1094.ch008>.
- [58] J. Řezáč and P. Hobza, *J. Chem. Theory Comput.* **9**, 2151 (2013), <http://dx.doi.org/10.1021/ct400057w>.
- [59] D. G. Truhlar, *Chem. Phys. Lett.* **294**, 45 (1998).
- [60] M. Burkatzki, C. Filippi, and M. Dolg, *J. Chem. Phys.* **126**, 234105 (2007).
- [61] R. Jastrow, *Phys. Rev.* **98**, 1479 (1955).
- [62] N. D. Drummond, M. D. Towler, and R. J. Needs, *Phys. Rev. B* **70**, 235119 (2004).
- [63] C. J. Umrigar and C. Filippi, *Phys. Rev. Lett.* **94**, 150201 (2005).
- [64] N. D. Drummond and R. J. Needs, *Phys. Rev. B* **72**,

SUPPORTING INFORMATION

BINDING CURVE

- 085124 (2005).
- [65] T. Kato, *Comm. Pure Appl. Math.* **10**, 151 (1957).
- [66] C. J. Umrigar, M. P. Nightingale, and K. J. Runge, *J. Chem. Phys.* **99**, 2865 (1993).
- [67] Y. Zhao and D. Truhlar, *Theor. Chem. Acc.* **120**, 215 (2008).
- [68] S. H. Vosko, L. Wilk, and M. Nusair, *Can. J. Phys.* **58**, 1200 (1980), <http://dx.doi.org/10.1139/p80-159>.
- [69] J. P. Perdew, K. Burke, and M. Ernzerhof, *Phys. Rev. Lett.* **77**, 3865 (1996).
- [70] C. Lee, W. Yang, and R. G. Parr, *Phys. Rev. B* **37**, 785 (1988).
- [71] A. D. Becke, *J. Chem. Phys.* **98**, 5648 (1993).
- [72] P. J. Stephens, F. J. Devlin, C. F. Chabalowski, and M. J. Frisch, *J. Phys. Chem.* **98**, 11623 (1994), <http://dx.doi.org/10.1021/j100096a001>.
- [73] A. Kumar and W. J. Meath, *Mol. Phys.* **75**, 311 (1992), <http://dx.doi.org/10.1080/00268979200100251>.
- [74] H. B. G. Casimir and D. Polder, *Phys. Rev.* **73**, 360 (1948).
- [75] A. Jiemchoorj, P. Norman, and B. E. Sernelius, *J. Chem. Phys.* **123**, 124312 (2005), <http://dx.doi.org/10.1063/1.2035589>.
- [76] M. A. L. Marques, A. Castro, G. Mallocci, G. Mulas, and S. Botti, *J. Chem. Phys.* **127**, 014107 (2007), <http://dx.doi.org/10.1063/1.2746031>.
- [77] R. Podeszwa, R. Bukowski, and K. Szalewicz, *J. Phys. Chem. A* **110**, 10345 (2006), <http://dx.doi.org/10.1021/jp064095o>.
- [78] V. Parsegian and B. Ninham, *Nature* **224**, 1197 (1969).
- [79] B. Ninham and V. Parsegian, *Biophys. J.* **10**, 646 (1970).
- [80] Y. C. Park, and J. S. Lee, *J. Phys. Chem. A* **110**, 5091 (2006), <http://dx.doi.org/10.1021/jp0582888>.
- [81] S. Azadi and R. E. Cohen, *J. Chem. Phys.* **143**, 104301 (2015), <http://dx.doi.org/10.1063/1.4930137>.
- [82] R. A. Buckingham, *Proc. R. Soc. London A: Math. Phys. Eng. Sci.* **168**, 264 (1938), NoStop
- [83] P. Hobza, H. L. Selzle, and E. W. Schlag, *J. Phys. Chem.* **100**, 18790 (1996), <http://dx.doi.org/10.1021/jp961239y>.
- [84] W. M. Haynes, ed., *CRC Handbook of Chemistry and Physics. 94th Edition* (CRC Press LLC, 2013-2014) pp. 3-34.
- [85] O. Bludský, M. Rubeš, P. Soldán, and P. Nachtigall, *J. Chem. Phys.* **128**, 114102 (2008), <http://dx.doi.org/10.1063/1.2890968>.
- [86] K. Nakano, K. Hongo, and R. Maezono, *Sci. Rep.* **6**, 29661 (2016).

For most of practical cases, we cannot expect the molecular dimer system to be accommodated within the possible size to be described by accurate basis sets, such as 'triple- ζ '(TZ) cc-pVTZ. In the present case actually, 'double- ζ '(DZ), cc-pVDZ, is the upper limit of the size even on the memory capacity of commercial supercomputers. For such a case, several schemes to correct biases due to less accurate basis sets are available. Schemes for basis set superposition error (BSSE) [1] corrects the 'unbalanced' accuracies to describe monomers and dimers, when they are used together to get binding energies. For an implementation of BSSE, we used here the counterpoise method. [2, 3] Schemes of the complete basis set (CBS) [4] were used to estimate an extrapolation to an enough large basis set.

Except for CCSD(T), we applied a CBS scheme by Truhlar [4] to get the corrected binding energy, ΔE_{CBS} , by the weighting as,

$$\Delta E_{\text{CBS}} = \frac{3^\gamma}{3^\gamma - 2^\gamma} \Delta E_3 - \frac{2^\gamma}{3^\gamma - 2^\gamma} \Delta E_2, \quad (\text{S-1})$$

where $\Delta E_{2,3}$ denote the energies evaluated by different basis set levels. For more reliability, we examined two different pairs for the correction, 'CBS': [(2,3) = (cc-pVDZ(DZ),cc-pVTZ(TZ))], and 'aCBS': [(2,3) = (aug-cc-pVDZ(aDZ),aug-cc-pVTZ(aTZ))]. The exponent, γ , is chosen as 3.4 (2.2) for HF and B3LYP-GD3 (MP2) as proposed by Truhlar *et al.*, [4] which is reported to be working well for non-covalent systems. [5]

For CCSD(T), the calculation was too costly to be done with larger basis sets other than cc-pVDZ level, making Truhlar's scheme not applicable to this case. Instead, we hence employed Sherrill's scheme [6],

$$\Delta E_{\text{CBS}}^{\text{CCSD(T)}} \approx \Delta E_{\text{CBS}}^{\text{MP2}} + \left(\Delta E^{\text{CCSD(T)}} - \Delta E^{\text{MP2}} \right)_{\text{cc-pVDZ}}, \quad (\text{S-2})$$

in which the extrapolation can be estimated only within a basis set, but assisted by further MP2 evaluations.

Binding curves of Sandwich (Type-A), T-shape (Type-B), and Parallel (Type-C) dimer configurations are shown in Fig. S-1. For SCF and correlated methods, we used Gaussian 09 [7] and the corresponding input files are attached to the end of this document. For DMC/B3LYP results, all the total energies are given in the next section. Comparisons of binding curves with/without corrections are summarized in Figs. S-2, S-3 and S-4 for SCF (HF and DFT in the following context), MP2, and CCSD(T), respectively. In each figure, panel (a) represents the final results, while (b)-(d) show separated contributions to (a): In panels (b), the amount of BSSE corrections

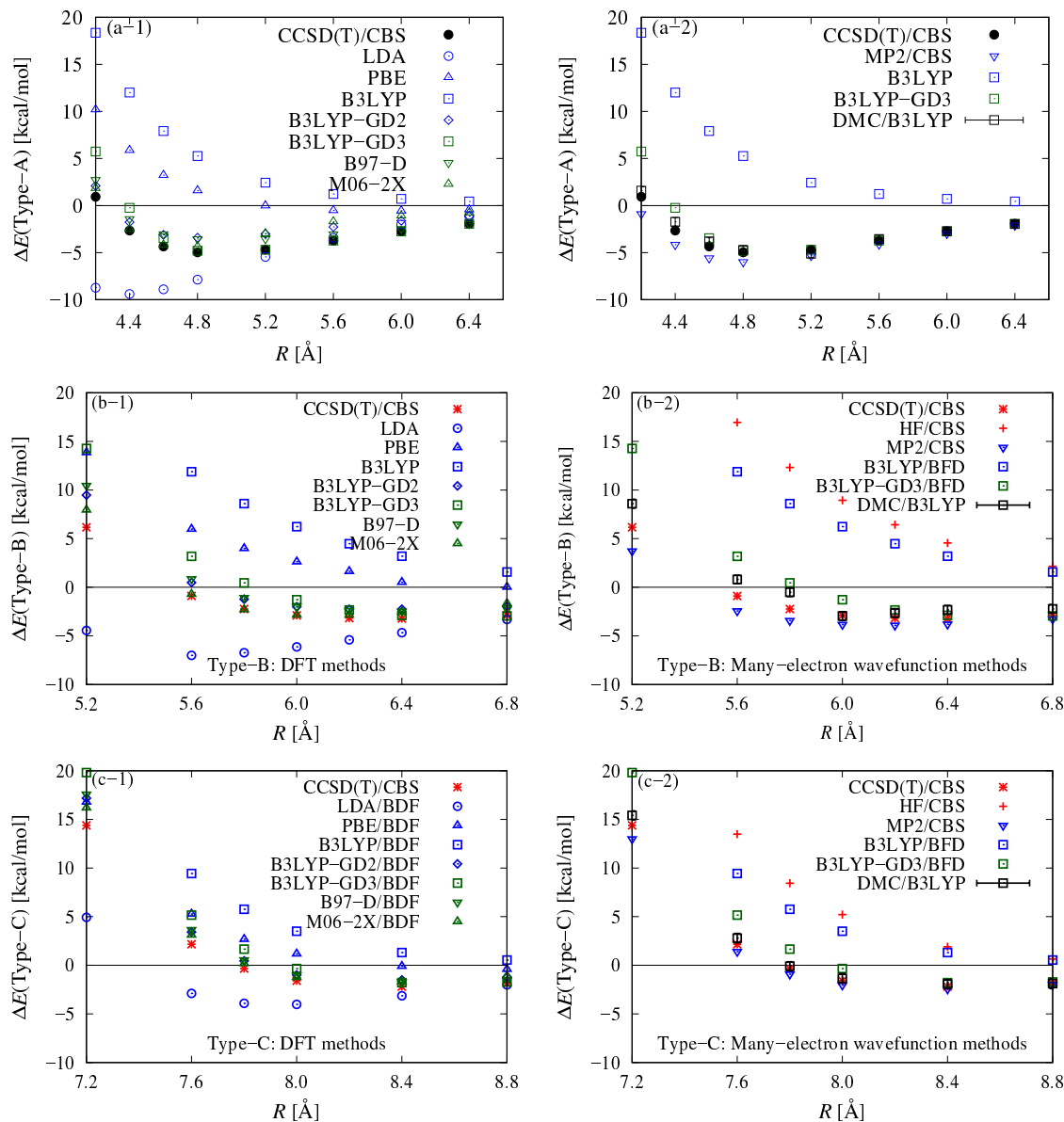


FIG. S-1. Binding curves for Sandwich (Type-A) [panels (a)], T-Shape (Type-B) [panels (b)], and Parallel (Type-C) [panels (c)], evaluated by several DFT [panel (a/b/c-1)] and correlated methods [panel (a/b/c-2)]. Results are corrected by CBS scheme if applicable. DMC results are evaluated using B3LYP/BDF-VTZ fixed nodes.

is found to increase as binding lengths gets shorter, because of the more overlapping, as expected. We see the more accurate basis sets used, the smaller the amount of the BSSE correction. Comparing panels (a) among the methods, we can see that correlated methods such as MP2 and CCSD(T) gives almost twice larger BSSE corrections than SCF methods. Comparison between panel (c) and (d) within each figure, we see that the dependence on basis sets gets weakened when BSSE corrections are applied. For SCF (Fig. S-2), the dependence seems almost completely disappeared, while for MP2 (Fig. S-3) there still remains the dependence especially on the

predictions of the binding length. In SCF methods, the energy approaches to the CBS limit always from bottom, while in MP2 it is alternating, namely the energy by DZ/TZ is above the limit but below by more improved basis set, aDZ/aTZ. In Fig. S-2 (a), we can also confirm that the BFD-VTZ result is quite close to the CBS limit, supporting a confidence about the present DMC using this basis set.

The larger BSSE corrections for correlated methods (MP2 and CCSD(T)) than those for SCF. This can be explained as follows: Since the correction should be zero

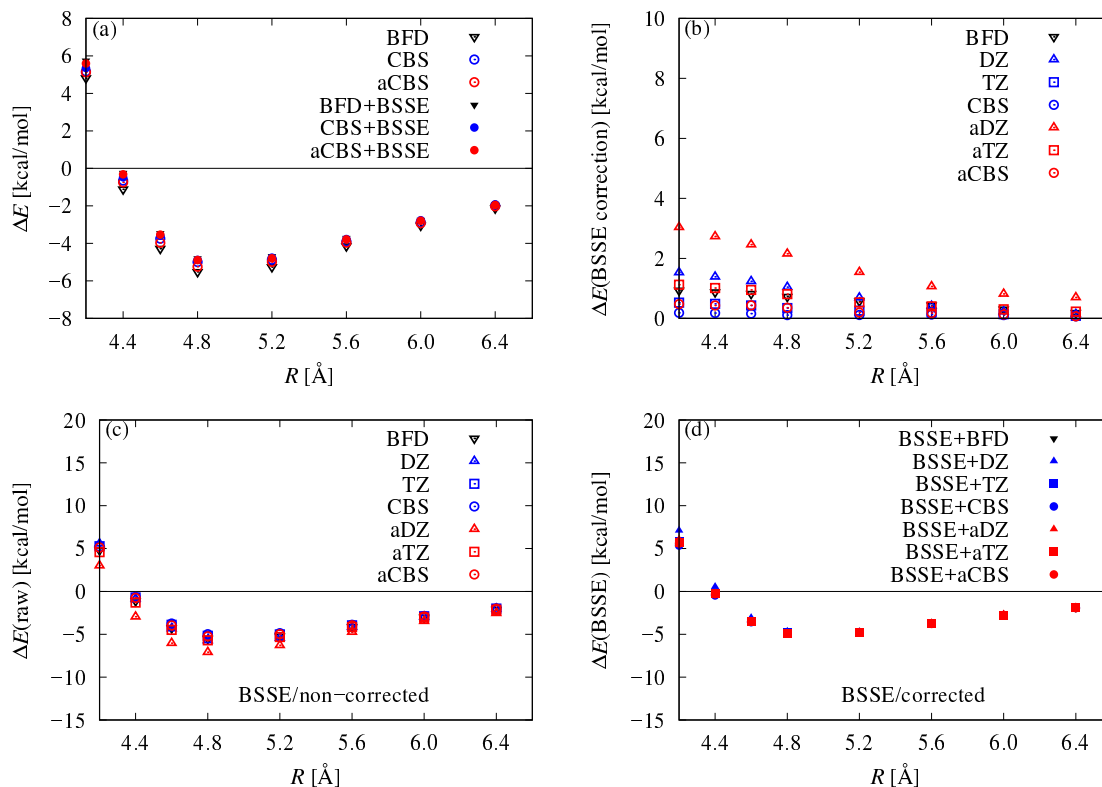


FIG. S-2. Binding curves and corrections for Type-A by B3LYP-GD3. Panel (a) shows the final binding curves after possible corrections, while (b)-(d) are separated contributions and comparisons with/without BSSE corrections. CBS (aCBS) stands for the CBS limit estimated by DZ/TZ (aDZ/aTZ) basis sets.

in the CBS limit, the amount of the correction would be a measure how far the basis set adopted is from CBS limit in the sense of the accuracy in each method. Suppose a basis set being sufficient to describe occupied orbitals used in SCF, but it is not the case also for further unoccupied orbitals in general, which are used in correlated methods such as CCSD(T) or MP2. The BSSE corrections with the same basis set is then getting larger for correlated methods than for SCF.

NODAL SURFACE DEPENDENCE AND TIME-STEP ERRORS

For the present DMC results, we have to examine the biases due to the approximations we applied, namely, the time-step approximation [8] and the fixed-node approximation. [9] In the sense of finite discretization of propagations, the smaller time-step, δt , would be reliable, but too small step cannot achieve such a random walk covering over the sampling space within a limited number of steps by a tractable computation. Fig. S-5 shows the time-step (δt) dependence of the DMC binding curves, evaluated for Type-A using B3LYP nodal surfaces. The

curves seem to be converging within errorbars, justifying the present choice of $\delta t = 0.02$ with enough high acceptance ratio being more than 99.5%.

The dependence of the binding curve (Type-A/ $\delta t = 0.02$) on the nodal surfaces is shown in Fig. S-5 (b) in absolute energy values, from which we can identify which nodal surface gives the variationally best estimation.[9] We noted that T -move scheme [10] is used in the present study to preserve the variational principle even under the locality approximation [11] for pseudo potentials. The choice of the nodal surfaces hardly changes the global shape such as the binding length. We also see that B3LYP nodes gives the variationally best description. Though there is still not enough convincing explanations, B3LYP nodes for DMC are also reported as the best for several other systems. [12–15]

All the DMC/B3LYP total energies with statistical errors are listed in Tables S-VIII. To compute binding energies, the reference is chosen at $R = 12.0$ Å for all the cases. They are depicted in Fig. S-1. In this table, under bars in R values indicate that the corresponding binding energies are used for the log-fitting shown in Figure 8 (see Appendix D).

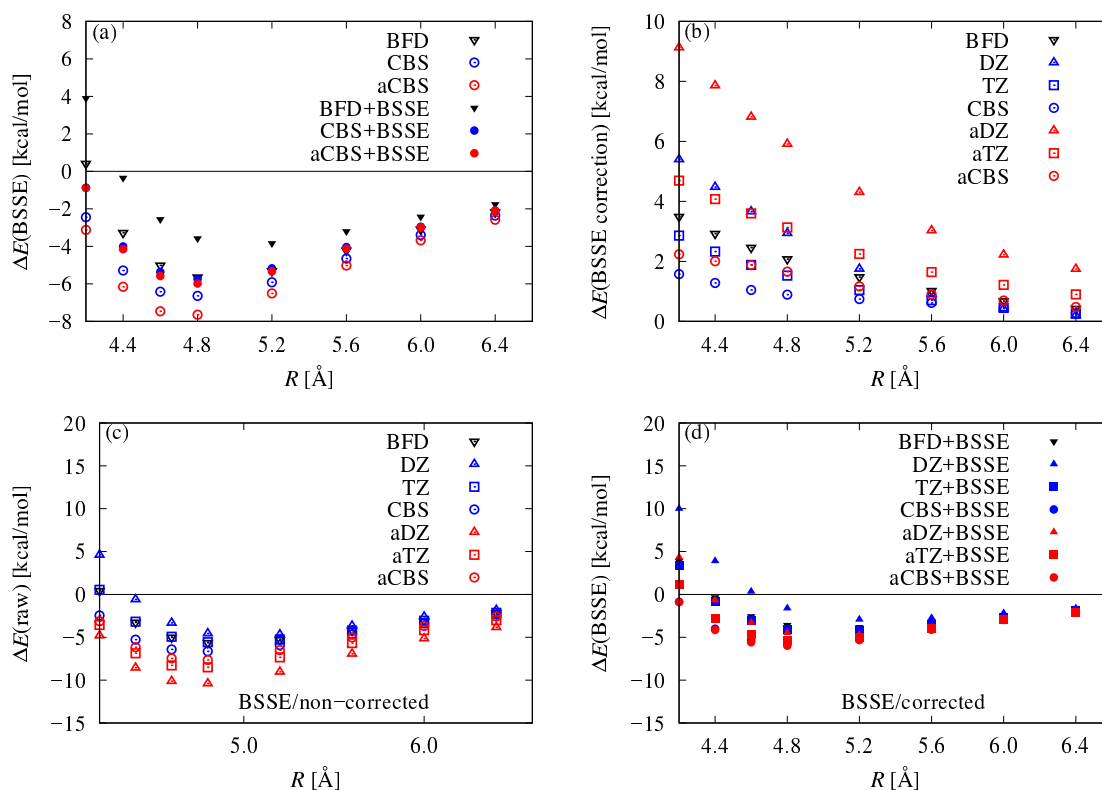


FIG. S-3. Binding curves and corrections for Type-A by MP2. Panel (a) shows the final binding curves after possible corrections, while (b)-(d) are separated contributions and comparisons with/without BSSE corrections. CBS (aCBS) stands for the CBS limit estimated by DZ/TZ (aDZ/aTZ) basis sets.

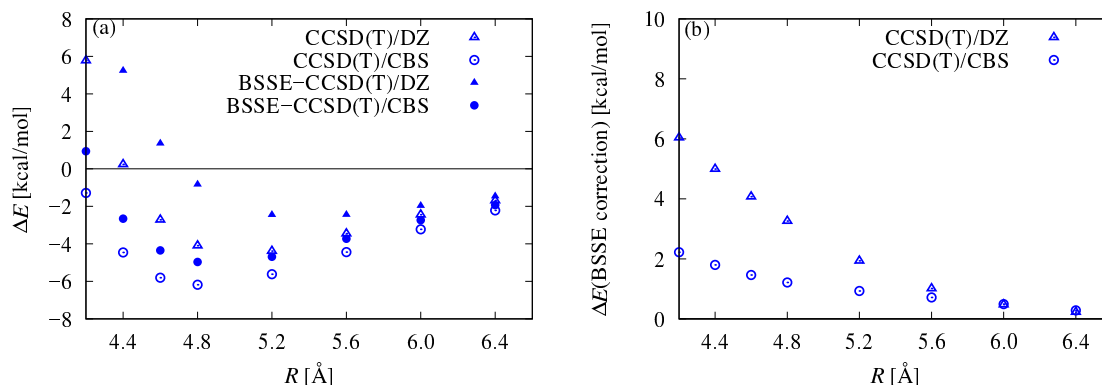


FIG. S-4. Binding curves and corrections for Type-A by CCSD(T). Panel (a) shows the final binding curves after possible corrections, while (b) shows the amount of BSSE contributions. 'CCSD(T)/DZ[CBS]' stands for the raw value without any corrections by DZ basis sets [CBS limit], while 'BSSE-CCSD(T)/DZ[CBS]' means that with BSSE corrections.

* kenta_hongo@mac.com

† National Institute for Materials Science (NIMS), 1-2-1 Sengen, Tsukuba, Ibaraki 305-0047, Japan; PRESTO, JST, 4-1-8 Honcho, Kawaguchi, Saitama 332-0012, Japan

- [1] van Duijneveldt, F. B.; van Duijneveldt-van de Rijdt, J. G. C. M.; van Lenthe, J. H. State of the Art in Counterpoise Theory. *Chemical Reviews* **1994**, *94*, 1873–1885.
- [2] Boys, S.; Bernardi, F. The calculation of small molecular interactions by the differences of separate total energies. Some procedures with reduced errors. *Molecular Physics* **1970**, *19*, 553–566.

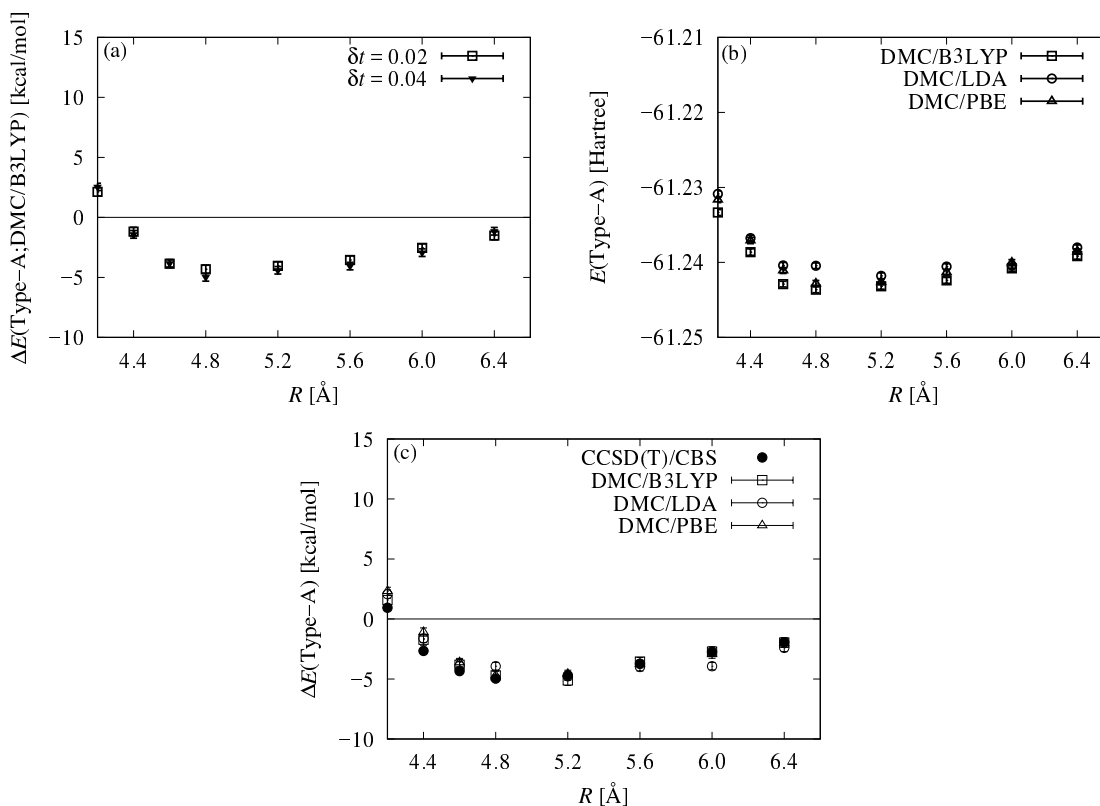


FIG. S-5. Time step dependence (left panel) and the nodal surface dependence (right panel) of the DMC binding curve for Type-A. For the left panel, DMC/B3LYP results are shown, which is variationally best in the right panel.

R	Sandwich	Error	R	T-Shape	Error	R	Parallel	Error
4.2	-61.23274	0.00050	5.2	-61.22226	0.00053	7.2	-61.21068	0.00049
4.4	-61.23801	0.00059	5.6	-61.23467	0.00046	7.6	-61.23080	0.00053
4.6	-61.24133	0.00053	5.8	-61.23676	0.00050	7.8	-61.23540	0.00049
4.8	-61.24275	0.00053	6.0	-61.24068	0.00051	8.0	-61.23738	0.00056
5.2	-61.24341	0.00052	6.2	-61.24018	0.00050	8.4	-61.23834	0.00048
5.4	-61.24324	0.00052	6.4	-61.23965	0.00052	8.8	-61.23824	0.00060
5.6	-61.24091	0.00049	6.8	-61.23950	0.00048	10.0	-61.23660	0.00051
6.0	-61.23959	0.00048	7.0	-61.23868	0.00052	11.0	-61.23578	0.00047
6.4	-61.23838	0.00049	8.0	-61.23775	0.00050	12.0	-61.23524	0.00056
6.6	-61.23798	0.00051	12.0	-61.23596	0.00052			
7.0	-61.23718	0.00046						
12.0	-61.23526	0.00043						

TABLE S-VIII. Total energies with statistical errors for Sandwich (Type-A), T-Shape (Type-B), and Parallel (Type-C) dimer configurations, evaluated from DMC/B3LYP with $\delta\tau = 0.02$. All energies and lengths are given in hartrees and angstroms, respectively.

- [3] Simon, S.; Duran, M.; Dannenberg, J. J. How does basis set superposition error change the potential surfaces for hydrogen-bonded dimers? *The Journal of Chemical Physics* **1996**, *105*, 11024–11031.
- [4] Truhlar, D. G. Basis-set extrapolation. *Chemical Physics Letters* **1998**, *294*, 45 – 48.
- [5] Šponer, J.; Jurečka, P.; Marchan, I.; Luque, F. J.; Orozco, M.; Hobza, P. Nature of Base Stacking: Reference Quantum-Chemical Stacking Energies in Ten Unique B-DNA Base-Pair Steps. *Chemistry – A European Journal* **2006**, *12*, 2854–2865.
- [6] Sinnokrot, M. O.; Sherrill, C. D. Highly Accurate Coupled Cluster Potential Energy Curves for the Benzene Dimer: Sandwich, T-Shaped, and Parallel-Displaced Configurations. *The Journal of Physical Chemistry A* **2004**, *108*, 10200–10207.
- [7] Frisch, M. J. et al. Gaussian 09 Revision D.01. Gaussian Inc. Wallingford CT 2009.
- [8] Umrigar, C. J.; Nightingale, M. P.; Runge, K. J. A diffusion Monte Carlo algorithm with very small timestep

- errors. *The Journal of Chemical Physics* **1993**, *99*, 2865–2890.
- [9] Reynolds, P. J.; Ceperley, D. M.; Alder, B. J.; Lester, W. A. Fixed-node quantum Monte Carlo for molecules. *The Journal of Chemical Physics* **1982**, *77*, 5593–5603.
- [10] Casula, M. Beyond the locality approximation in the standard diffusion Monte Carlo method. *Phys. Rev. B* **2006**, *74*, 161102.
- [11] Mitáš, L.; Shirley, E. L.; Ceperley, D. M. Nonlocal pseudopotentials and diffusion Monte Carlo. *The Journal of Chemical Physics* **1991**, *95*, 3467–3475.
- [12] Hongo, K.; Cuong, N. T.; Maezono, R. The Importance of Electron Correlation on Stacking Interaction of Adenine-Thymine Base-Pair Step in B-DNA: A Quantum Monte Carlo Study. *Journal of Chemical Theory and Computation* **2013**, *9*, 1081–1086.
- [13] Hongo, K.; Maezono, R. A benchmark quantum Monte Carlo study of the ground state chromium dimer. *International Journal of Quantum Chemistry* **2012**, *112*, 1243–1255.
- [14] Kolorenč, J.; Hu, S.; Mitas, L. Wave functions for quantum Monte Carlo calculations in solids: Orbitals from density functional theory with hybrid exchange-correlation functionals. *Phys. Rev. B* **2010**, *82*, 115108.
- [15] Per, M. C.; Walker, K. A.; Russo, S. P. How Important is Orbital Choice in Single-Determinant Diffusion Quantum Monte Carlo Calculations? *Journal of Chemical Theory and Computation* **2012**, *8*, 2255–2259.

```

%chk=chs.chk
%mem=64000MB
%nprocshared=32
#p b3lyp/cc-pVTZ guess=huckel sp counterpoise=2
empiricaldispersion=gd3

```

BSSE B3LYP-GD3/cc-pVTZ calculation of cyclohexasilane; Type-A; R = 5.2

```

0 1 0 1 0 1
Si(Fragment=1) -2.224812139 -1.097382683 -6.250213335
Si(Fragment=1) -1.041812139 -3.171382683 -6.055213335
Si(Fragment=1) 1.063187861 -2.873382683 -4.951213335
Si(Fragment=1) 2.393187861 -1.211382683 -6.049213335
Si(Fragment=1) 1.210187861 0.862617317 -6.244213335
Si(Fragment=1) -0.893812139 0.564617317 -7.348213335
H(Fragment=1) -2.573812139 -0.608382683 -4.875213335
H(Fragment=1) -3.509812139 -1.304382683 -6.995213335
H(Fragment=1) -1.876812139 -4.172382683 -5.312213335
H(Fragment=1) -0.794812139 -3.720382683 -7.429213335
H(Fragment=1) 1.805187861 -4.175382683 -4.896213335
H(Fragment=1) 0.812187861 -2.437382683 -3.537213335
H(Fragment=1) 2.742187861 -1.700382683 -7.424213335
H(Fragment=1) 3.679187861 -1.004382683 -5.304213335
H(Fragment=1) 2.045187861 1.863617317 -6.986213335
H(Fragment=1) 0.963187861 1.411617317 -4.870213335
H(Fragment=1) -0.642812139 0.128617317 -8.761213335
H(Fragment=1) -1.636812139 1.866617317 -7.403213335
Si(Fragment=2) -3.008471290 0.549438822 -1.380525741
Si(Fragment=2) -1.825471290 -1.524561178 -1.185525741
Si(Fragment=2) 0.279528710 -1.226561178 -0.081525741
Si(Fragment=2) 1.609528710 0.435438822 -1.179525741
Si(Fragment=2) 0.426528710 2.509438822 -1.374525741
Si(Fragment=2) -1.677471290 2.211438822 -2.478525741
H(Fragment=2) -3.357471290 1.038438822 -0.005525741
H(Fragment=2) -4.293471290 0.342438822 -2.125525741
H(Fragment=2) -2.660471290 -2.525561178 -0.442525741
H(Fragment=2) -1.578471290 -2.073561178 -2.559525741
H(Fragment=2) 1.021528710 -2.528561178 -0.026525741
H(Fragment=2) 0.028528710 -0.790561178 1.332474259
H(Fragment=2) 1.958528710 -0.053561178 -2.554525741
H(Fragment=2) 2.895528710 0.642438822 -0.434525741
H(Fragment=2) 1.261528710 3.510438822 -2.116525741
H(Fragment=2) 0.179528710 3.058438822 -0.000525741
H(Fragment=2) -1.426471290 1.775438822 -3.891525741
H(Fragment=2) -2.420471290 3.513438822 -2.533525741

```

```
%chk=chs.chk
%mem=64000MB
%nprocshared=16
#p mp2/aug-cc-pVTZ guess=huckel sp counterpoise=2
```

BSSE MP2/aug-cc-pVTZ calculation of cyclohexasilane; Type-B; R = 6.0

```
0 1 0 1 0 1
Si(Fragment=1) -2.083754109 -1.338812346 -6.998954188
Si(Fragment=1) -0.900754109 -3.412812346 -6.803954188
Si(Fragment=1) 1.204245891 -3.114812346 -5.699954188
Si(Fragment=1) 2.534245891 -1.452812346 -6.797954188
Si(Fragment=1) 1.351245891 0.621187654 -6.992954188
Si(Fragment=1) -0.752754109 0.323187654 -8.096954188
H(Fragment=1) -2.432754109 -0.849812346 -5.623954188
H(Fragment=1) -3.368754109 -1.545812346 -7.743954188
H(Fragment=1) -1.735754109 -4.413812346 -6.060954188
H(Fragment=1) -0.653754109 -3.961812346 -8.177954188
H(Fragment=1) 1.946245891 -4.416812346 -5.644954188
H(Fragment=1) 0.953245891 -2.678812346 -4.285954188
H(Fragment=1) 2.883245891 -1.941812346 -8.172954188
H(Fragment=1) 3.820245891 -1.245812346 -6.052954188
H(Fragment=1) 2.186245891 1.622187654 -7.734954188
H(Fragment=1) 1.104245891 1.170187654 -5.618954188
H(Fragment=1) -0.501754109 -0.112812346 -9.509954188
H(Fragment=1) -1.495754109 1.625187654 -8.151954188
Si(Fragment=2) 1.275166713 0.786100526 -2.228723699
Si(Fragment=2) 0.554936428 2.042475603 -0.320378866
Si(Fragment=2) -1.017668521 0.803836125 0.995421620
Si(Fragment=2) -2.880117780 0.082571378 -0.326625248
Si(Fragment=2) -2.159887495 -1.173803699 -2.234970081
Si(Fragment=2) -0.588201835 0.064693179 -3.550403725
H(Fragment=2) 2.030674087 -0.421119680 -1.756098073
H(Fragment=2) 2.212674257 1.607052745 -3.063119325
H(Fragment=2) 1.737849632 2.428780005 0.517929109
H(Fragment=2) -0.097880578 3.308476064 -0.790866688
H(Fragment=2) -1.493938169 1.636341792 2.148198501
H(Fragment=2) -0.330386782 -0.402989647 1.564375368
H(Fragment=2) -3.635625154 1.289791585 -0.799250873
H(Fragment=2) -3.818544612 -0.738523441 0.508137220
H(Fragment=2) -3.342433857 -1.560756239 -3.072610715
H(Fragment=2) -1.507070489 -2.439804159 -1.764482259
H(Fragment=2) -1.275116732 1.270870812 -4.118690132
H(Fragment=2) -0.111012898 -0.767669888 -4.703547447
```

```
%chk=chs.chk
%mem=64000MB
%nprocshared=32
#p b3lyp/gen guess=huckel pseudo=read sp counterpoise=2
```

BSSE B3LYP/BFD calculation of cyclohexasilane; Type-C; R = 8.0

```
0 1 0 1 0 1
Si(Fragment=1) 0.615686612 -2.091625189 -5.441864161
Si(Fragment=1) 1.798686612 -4.165625189 -5.246864161
Si(Fragment=1) 3.903686612 -3.867625189 -4.142864161
Si(Fragment=1) 5.233686612 -2.205625189 -5.240864161
Si(Fragment=1) 4.050686612 -0.131625189 -5.435864161
Si(Fragment=1) 1.946686612 -0.429625189 -6.539864161
H(Fragment=1) 0.266686612 -1.602625189 -4.066864161
H(Fragment=1) -0.669313388 -2.298625189 -6.186864161
H(Fragment=1) 0.963686612 -5.166625189 -4.503864161
H(Fragment=1) 2.045686612 -4.714625189 -6.620864161
H(Fragment=1) 4.645686612 -5.169625189 -4.087864161
H(Fragment=1) 3.652686612 -3.431625189 -2.728864161
H(Fragment=1) 5.582686612 -2.694625189 -6.615864161
H(Fragment=1) 6.519686612 -1.998625189 -4.495864161
H(Fragment=1) 4.885686612 0.869374811 -6.177864161
H(Fragment=1) 3.803686612 0.417374811 -4.061864161
H(Fragment=1) 2.197686612 -0.865625189 -7.952864161
H(Fragment=1) 1.203686612 0.872374811 -6.594864161
Si(Fragment=2) -6.992746775 0.152866824 -6.526224468
Si(Fragment=2) -5.830540937 -1.932914660 -6.331845484
Si(Fragment=2) -3.726457319 -1.657711131 -5.220206988
Si(Fragment=2) -2.376764792 -0.006306257 -6.310133604
Si(Fragment=2) -3.538970631 2.079475227 -6.504512587
Si(Fragment=2) -5.642054302 1.804262008 -7.616147761
H(Fragment=2) -7.341591259 0.642252232 -5.151322126
H(Fragment=2) -8.277192653 -0.040062209 -7.275941865
H(Fragment=2) -6.677672819 -2.927380895 -5.593821445
H(Fragment=2) -5.584275356 -2.481310986 -7.706218336
H(Fragment=2) -2.997285886 -2.966955162 -5.165598487
H(Fragment=2) -3.977950474 -1.222356939 -3.806095635
H(Fragment=2) -2.027920309 -0.495691666 -7.685035946
H(Fragment=2) -1.091318967 0.186613086 -5.560412884
H(Fragment=2) -2.691842092 3.073939299 -7.241536635
H(Fragment=2) -3.785236212 2.627871552 -5.130139736
H(Fragment=2) -5.390564489 1.368905654 -9.029259123
H(Fragment=2) -6.372225682 3.113515728 -7.670759585

H 0
s 9 1.00
0.013000 0.000706
0.029900 -0.002119
0.068770 0.057693
0.158170 0.230695
0.363792 0.277612
0.836721 0.169833
1.924458 0.097443
```

4.426254	0.029966
10.180385	-0.000452
s 1 1.00	
0.170654	1.000000
p 9 1.00	
0.003000	0.001242
0.007800	-0.000913
0.020281	-0.000054
0.052730	-0.000238
0.137097	-0.011530
0.356451	-0.018235
0.926774	-0.013929
2.409612	-0.009395
6.264991	-0.000347
p 1 1.00	
0.495357	1.000000
d 1 1.00	
0.955745	1.000000

Si 0	
s 9 1.00	
0.059887	0.167492
0.130108	0.532550
0.282668	0.464290
0.614115	-0.002322
1.334205	-0.268234
2.898645	0.031921
6.297493	-0.000106
13.681707	-0.000145
29.724387	0.000067
s 1 1.00	
0.090113	1.000000
s 1 1.00	
0.507467	1.000000
p 9 1.00	
0.036525	0.078761
0.076137	0.308331
0.158712	0.417773
0.330843	0.281676
0.689658	0.069876
1.437625	-0.056306
2.996797	0.000744
6.246966	-0.000259
13.022097	-0.000022
p 1 1.00	
0.056148	1.000000
p 1 1.00	
0.146758	1.000000
d 1 1.00	
0.170395	1.000000
d 1 1.00	
0.539756	1.000000
f 1 1.00	
0.352999	1.000000

H 0

QMC 0 0

COMMENT LINE

3

1 4.47692410 1.00000000

3 2.97636451 4.47692410

2 3.01841596 -4.32112340

Si 0

QMC 2 10

COMMENT LINE

3

1 1.80721061 4.00000000

3 9.99633089 7.22884246

2 2.50043232 -13.06725590

COMMENT LINE

1

2 2.26686403 21.20531613

COMMENT LINE

1

2 2.11659661 15.43693603